AN ABSTRACT OF THE THESIS OF

Satish P. Serchan for the degree of Master of Science in Water Resources Science presented on February 03, 2021.

Title: Evidence of Buried Particulate Organic Carbon as Foundation for Heterotrophic Carbon Metabolism in the Hyporheic Zone of a Montane Headwater Stream in the H. J. Andrews Experimental Forest, Oregon, USA

Abstract approved: _____

Steven M. Wondzell

Streams and rivers play a critical role in global carbon (C) cycling by processing, storing, and transporting C. Headwater streams which make up more than 95% of the length of streams and rivers worldwide have disproportionate influence on fluvial C dynamics. The hyporheic zone (HZ) of headwater streams is a critical site where organic C is processed and the hyporheic exchange flow (HEF) plays crucial role in cycling of C. This study investigated the metabolism of stream-source dissolved organic carbon (DOC_{st}) and buried particulate organic carbon (POC_b) in the hyporheic zone of a small mountain headwater stream. We designed hyporheic mesocosms to stimulate near-stream hyporheic flow paths located in the HZ of Watershed 1 located in the H. J. Andrews Experimental Forest. We then investigated the metabolism of C in the hyporheic mesocosm and compared the results from the mesocosm to those from a hyporheic well network located in the riparian zone of Watershed 1. We examined three questions:

1. What is the source of metabolic C substrate for hyporheic metabolism in the hyporheic zone?
2. What factors influence metabolism in the hyporheic zone?
3. How do the rate coefficients from hyporheic mesocosm compare to rate coefficients from the near-stream hyporheic flow paths measured in the well network?

Evidence of Buried Particulate Organic Carbon as Foundation for Heterotrophic Carbon Metabolism in the Hyporheic Zone of a Montane Headwater Stream in the H.J. Andrews Experimental Forest, Oregon, USA

by

Satish P. Serchan

A THESIS

submitted to

Oregon State University

in partial fulfillment of
the requirements for the
degree of

Master of Science

Presented February 03, 2021

Commencement June 2021

Master of Science thesis of Satish P. Serchan presented on February 03, 2021

APPROVED:

Major Professor, representing Water Resources Science

Director of the Water Resources Graduate Program

Dean of the Graduate School

I understand that my thesis will become part of the permanent collection of Oregon State University libraries. My signature below authorizes release of my thesis to any reader upon request.

Satish P. Serchan, Author

ACKNOWLEDGMENTS

I would like to express my deepest appreciation to my advisor, Dr. Steve Wondzell, for expertly guiding me through my graduate education at Oregon State University. Thank you for accepting me as a graduate student in Water Resources Graduate Program and giving me an opportunity to do my research work at the H.J. Andrews Experimental Forest. Thank you, Steve, for weekly meetings, for your thorough comments and feedbacks on my proposals, drafts, and writing assignments. They have helped me become a concise writer and a thinker. Your guidance in literature review helped me summarize scientific literatures in succinct and lucid manner. Thank you for guiding me through every aspect of scientific research. You have helped me with design of research experiments, data collection, and analysis. Thank you for including me in the Stream Carbon Team and introducing me to all the principal investigators of the Stream Carbon Team: Dr. Roy Haggerty, Dr. Kevin Feris, and Dr. Daniele Tonina.

I am genuinely appreciative of Dr. Roy Haggerty for his support, guidance, and including me in his research team. I deeply appreciate Roy's crucial inputs during early stages of mesocosm designs. His suggestions, guidance, and hard work during field operations of mesocosms helped establish mesocosm facility at the H.J. Andrews Experimental Forest. Thank you to Dr. Kevin Feris for his availability for meetings during design phase of mesocosms. His guidance, ideas, and knowledge helped with designing sample collection from the mesocosms. Thank you to Robert Pennington, Angelo Sanfilippo, Chong Seok Choi, Jeff Reeder, and Karla Jarecke for helping with field work at the H. J. Andrews. I enjoyed your company in the field.

Thank you to Dr. Mary Santelmann for giving me an opportunity to be part of Water Resources Graduate Program. Thank you for your words of encouragement and being so enthusiastic about my research project. I am also extremely grateful to my committee, Dr. Roy Haggerty, Dr. Lisa Ganio, Dr. Jeff Hatten, and Dr. Kevin Feris for their assistance and providing sound advice during meetings. Thank you for your availability and your guidance. Thank you to Ariel Muldoon for helping me understand statistical analysis and providing guidance to statistical model analysis of my data.

I am extremely appreciative of Kathy Motter at the Oregon State University Institute for Water and Watersheds Collaboratory, for providing generous laboratory space to conduct

chemical analyses on all samples collected for this research. Thank you, Kathy for training me how to use all instruments needed for my research. I am grateful for Kathy's availability, and professionalism in answering my questions about instruments and understanding chemical analyses reports.

I take this opportunity to record my sincere thanks to Roy and Steve for providing funding for this research. Thank you, Roy for graduate research assistantship. Thank you to the PNW Research Station for giving me office space and lab space. Thank you to Bob Barrus, Brenda Gay, and Dan Merner at PNW Research Station with providing crucial assistance in the office. Thank you for every member of the H.J. Andrews Experimental Forest - Long Term Ecological Research group for support, friendship, and encouraging me. I enjoyed participating in monthly meetings. Thank you, Lina DiGregorio for giving me an opportunity to serve as a graduate student representative. Thank you, Dr. Chelsea Batavia, for friendship and serving as a co-representative with me on HJA-LTER graduate student representative committee.

I would also like to express my gratitude to Mark Schulze, Kathy Keable, Kathleen Turnley, Adam Kennedy, Greg Downing, and Terry Cryer for their helping hand in this venture. I would also like to thank the entire staff at the H. J. Andrews Experimental Forest and PNW Research Station for maintaining the research facilities and providing data necessary for this research project. I would also like to express my gratitude to Dr. Tyler Radniecki and his research group for allowing me to use spaces in their laboratory.

I would also like to express my gratitude to the administrative support staff of Water Resources Graduate Program. Thank you to Jennifer Cohen, Annie Ingersoll, Amy Zimmerman, and Catherine Mullins. Thank you to Michael and Nona Harrison, and Ben and Lynn Russell for friendship and making me feel at home in Corvallis. Thank you to Rakshya's and my family for providing support and words of encouragement throughout my graduate school. Thank you to Deane and Becky Wang and, above all, I am indebted to Rakshya Gauchan for supporting me throughout this entire process.

CONTRIBUTION OF AUTHORS

Dr. Steve Wondzell assisted with study design, analysis, and edits. Dr. Roy Haggerty and Dr. Kevin Feris assisted with mesocosm and study design.

TABLE OF CONTENTS

TABLE OF CONTENTS (Continued)

LIST OF FIGURES

Figure Page

LIST OF FIGURES (Continued)

Figure Page

LIST OF FIGURES (Continued)

Figure Page

LIST OF TABLES

LIST OF APPENDIX FIGURES

Figure Page

LIST OF APPENDIX TABLES

1 Introduction

Streams and rivers play a critical role in global carbon (C) cycling (Cole et al., 2007; Aufdenkampe et al., 2011). Once regarded as passive conduits for material transport between terrestrial and marine ecosystems, they are now recognized as biogeochemically important components of aquatic ecosystems that emit carbon dioxide (CO_2) to the atmosphere, store C in the floodplain, export substantial amount of C to downstream environments (Cole et al., 2007; Butman et al., 2016; Marx et al., 2017).

Headwater streams – first and second-order streams – comprise >95% of streams and river length worldwide (Downing et al., 2012) and have disproportionate influence on fluvial C dynamics (Marx et al., 2017). They are primary connectors between terrestrial and aquatic ecosystems. They receive, process, and transport substantial amount of C (Finlay, 2003; Johnson et al., 2008; Butman and Raymond, 2011; Argerich et al., 2016; Marx et al., 2017). Particulate and dissolved forms of organic C from terrestrial sources are primary forms of C input (Palmer et al., 2001; Richardson and Danehy, 2007). Headwater streams may transport some of this C to downstream environments, but higher proportions are processed (Marx et al., 2017). As a result, inorganic forms such as CO_2 evaded from the surface water to the atmosphere (Butman and Raymond, 2011), and DIC transported to downstream environments (Argerich et al., 2016) can be primary forms of C exports from headwater stream systems.

The hyporheic zone (HZ) can influence fluvial C dynamics in headwater streams. It can contribute DIC to the stream water (Corson-Rikert et al., 2016) and it can also be a biogeochemically active site where organic C is metabolized (Findlay et al., 1993). By

virtue of its location at the sediment-water interface, it integrates water from different sources such as stream water, groundwater, hillslope, and riparian soil water. Thus, the mixing of different source waters and their contact time with sediment in the HZ promote metabolism of organic C (Baker et al., 1999; Stegen et al., 2016) and/or contribute to elevated levels of DIC (Schindler and Krabbenhoft, 1998; Battin, 1999). Long-time scale groundwater flow paths can be present in the HZ and provide a source of DIC in gaining streams (Schindler and Krabbenhoft, 1998). In short flow paths, downwelling stream water can provide a steady supply of metabolic C substrates and dissolved oxygen (O_2) to fuel heterotrophic respiration (Findlay et al., 1993; Jones et al., 1995; Sobczak and Findlay, 2002).

Previous studies conducted at our study site showed that approximately one-third of stream DIC may be sourced from the HZ (Argerich et al., 2016) and the metabolism of buried POC (POC_b) within the hyporheic sediments may be a major process producing DIC (Corson-Rikert et al., 2016). In this study we use engineered systems to provide direct, quantitative estimates of C processing in the HZ. We use hyporheic mesocosms to examine O_2 and C dynamics along controlled flow paths which are isolated from other sources of water naturally occurring in the HZ.

2 Evidence of buried particulate organic carbon as foundation for heterotrophic carbon metabolism in the hyporheic zone of a montane headwater stream in the H. J. Andrews Experimental Forest, Oregon, USA

2.1 Abstract

Six 2-meter long hyporheic mesocosms were engineered to replicate near-stream short hyporheic flow paths in the valley floor of Watershed 1 at the H.J. Andrews Experimental Forest. Dissolved oxygen (O_2), stream-source dissolved organic carbon (DOC_{st}), and dissolved inorganic carbon (DIC) were measured at the inlet and outlet of the mesocosms on seven different dates over an eighteen-month period. The O_2 concentrations consistently declined along hyporheic flow paths with losses ranging from -0.179 mM to -0.016 mM, DIC consistently increased, ranging from 0.004 mM to 0.111 mM. Unlike O_2 and DIC, the concentrations of DOC_{st} did not change from the inlet to the outlet. Heterotrophic metabolism, as approximated by O_2 uptake rate coefficients (k_{O_2}), was two-fold higher on warmer compared to cooler sampling dates. Overall, the metabolism of DOC_{st} could explain 7% of O_2 consumed during Summer-Fall and 26% of O_2 loss during Winter-Spring. Clearly, POC_b is an important substrate for HZ metabolism. The relationship between DIC accumulation rate coefficient (k_{DIC}) estimated from the mesocosm and the time elapsed since packing of the mesocosm indicate that packing of mesocosm may have made POC_b bioavailable for heterotrophic metabolism. However, the bioavailable pool of POC_b tends to decline with time which is indicated by decline in k_{DIC} with time. Temperature positively influenced k_{O_2} with the magnitude of Summer-Fall k_{O_2} two times greater than Winter-Spring k_{O_2}.

The k_{O_2} was higher in the mesocosm compared to the well network. Also, the mesocosms showed large seasonal changes in k_{O_2} which were not observed in the well network. The biggest difference occurred during the summer when the k_{O_2} in the mesocosms was more than twice as high as that estimated from the well network. Two factors might explain this difference: 1) the Summer-Fall data include our first mesocosm sample after packing when k_{DIC} suggest that POC_b was more bioavailable, and 2) despite housing the mesocosms in an insulated box with a cold-water radiator through which stream water was pumped continuously, mesocosm temperatures were as much as 5 °C warmer than the stream and hyporheic zone during the summer and fall. The k_{DIC} from the mesocosm were generally lower than those estimated from the well network, although their ranges overlapped. The differences in k_{DIC} between the mesocosms and the well network were largest in during Winter-Spring which suggests that there may be additional sources of DIC, other than metabolism of DOC_{st} and POC_b at the well network.

2.2 Introduction

The hyporheic zone (HZ) – the near-stream aquifer where stream water moves from the surface channel into the subsurface and reemerges at downstream location over a relatively short period of time – is a critical site where organic carbon (C) is processed (Findlay et al., 1993; Battin, 1999; Corson-Rikert et al., 2016). The mixing of different source water and their contact time with metabolically active sediment stimulates oxidation of organic C (Stegen et al., 2016). Studies show both dissolved organic carbon (DOC) and particulate organic carbon (POC) are metabolized in the HZ (Grimm and Fisher, 1984; Findlay et al., 1993; Pusch, 1996; Baker et al., 1999; Brugger et al., 2001; Sobczak and Findlay, 2002; Burrows et al., 2017). This has two consequences: first, the HZ can be a sink for organic C within the stream environment (Battin et al., 2003); second, inorganic C generated from the metabolism of organic C can contribute dissolved inorganic carbon (DIC) to the stream (Corson-Rikert et al., 2016).

The C dynamics within the HZ vary with space and time due to the extent of mixing of different source waters (Schindler and Krabbenhoft, 1998; Battin, 1999; Baker et al., 2000) and biogeochemical processes that occur in the flood plain and the HZ (Findlay et al., 1993; Jones et al., 1995; Shibata et al., 2001; Corson-Rikert et al., 2016). The mixing of different sources of water in the HZ is generally controlled by interactions between geologic and hydrologic settings of streams (Cardenas and Wilson, 2006; Poole et al., 2006; Ward et al., 2012; Wondzell et al., 2013). As a result, the areal extent of the HZ fluctuates spatially and temporally (Malzone et al., 2016) and the hyporheic flow paths can occur over a wide range of spatial and temporal scales (Harvey and Bencala,

1993; Wondzell and Swanson, 1999; Kasahara and Wondzell, 2003; Ward et al., 2016). These variable factors will greatly impact biogeochemical processes in the HZ. Short-time scale hyporheic exchange flows (HEF) can provide continuous supply of dissolved oxygen (O_2) and allochthonous dissolved organic carbon (DOC) to the HZ which can stimulate metabolic activity within the hyporheic sediment (Findlay et al., 1993). In contrast, elevated levels of DIC can occur in the HZ from groundwater in gaining stream where metabolic activity along anoxic flow path is relatively slow due to anaerobic pathways of C metabolism (Hedin et al., 1998; Baker et al., 1999) which can also lead to production of DOC (Schindler and Krabbenhoft, 1998; Helton et al., 2015). The C fluxes from riparian and hillslope flow paths to streams can be seasonal (e.g., during snow melt in alpine streams; Battin, 1999) and C flushed from the shallow subsurface can stimulate hyporheic metabolism(?) (Baker et al., 2000). Similarly, soil CO_2 produced from root respiration and oxidation of organic matter in the vadose zone can contribute to DIC in the HZ as the height of water table in the floodplain responds to diurnal cycle of evapotranspiration (Shibata et al., 2001; Tsypin and Macpherson et al., 2012).

This study focuses on heterotrophic metabolism of DOC and POC in the HZ of a small mountain headwater stream located in the H.J. Andrews Experimental Forest, Oregon. The HZ at this site has been focus of many hyporheic studies (Kasahara and Wondzell, 2003; Wondzell, 2006; Argerich et al., 2016; Corson-Rikert et al., 2016; Ward et al., 2016). Previous investigation of C dynamics in the HZ demonstrated that the HZ is a metabolically active site for the oxidation of organic C and source of DIC to the stream

(Corson-Rikert et al., 2016). While quantifying whole stream C budget for the same site, Argerich et al., (2016) reported that one-third of stream DIC was sourced from the HZ.

Results from groundwater flow models calibrated to the water table elevations at the site to quantify HEF and residence times of stream water in the HZ indicated that step-pool sequences were primary drivers of HEF, approximately 76% of stream discharge, at baseflow conditions, flowed through the HZ within a 100-m reach, and the distribution of residence times of stream water in the HZ was highly skewed toward relatively short-residence-time hyporheic flow paths between 0 to 24 hours with a median residence time of 18 hours (Kasahara and Wondzell, 2003). Further analysis and results from other tracer studies conducted at range of base flow conditions have found strong persistence of floodplain water table elevations in the down valley direction indicating lateral inputs of shallow hillslope water or deep groundwater in the HZ (Wondzell, 2006; Voltz et al., 2013) may not strongly influence the site. Further analysis by Ward et al. (2016) at this site indicated that near-stream hyporheic flow paths were not influenced by stream discharge conditions or hydraulic gradients at stream-hyporheic-riparian-hillslope continuum. The tracer injected at upstream of the site (mixing-length) consistently arrived at the near-stream hyporheic flow paths within 20 hr (Figure 5 in Ward et al., 2016).

The objective of our study is to provide direct, quantitative field estimates of organic C processing and DIC production in the HZ. Specifically, we used hyporheic mesocosms, designed to simulate near-stream hyporheic flow paths, to examine the metabolism of stream-source DOC (DOC_{st}) and buried POC (POC_b). The design of the

hyporheic mesocosms created 100% stream water hyporheic flow paths isolated from the influences of riparian soils and drainage of solutes from the vadose zone as well as influences from hillslope or deeper groundwater (Figure 2.1). The mesocosms allowed us to investigate heterotrophic metabolism of DOC_{st} and POC_{b}, and the effect of factors such as water temperature and season on metabolic rate coefficients. Finally, we compared rate coefficients estimated from the mesocosms to rate coefficients calculated for the near-stream hyporheic flow paths at the well network to constrain processes controlling C dynamics in the HZ.

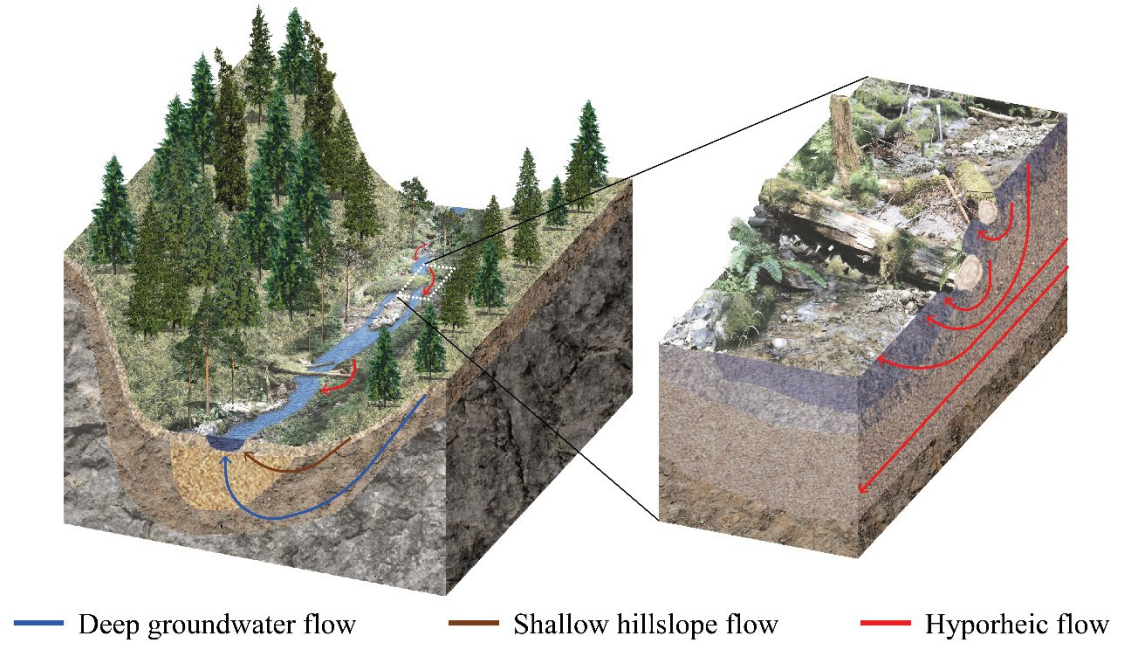

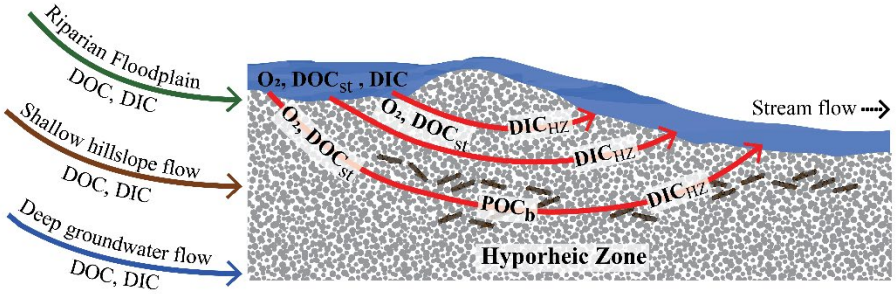

Figure 2.1– Conceptual diagram of flow paths at watershed scale and nested hyporheic flow paths at a reach scale (top panel). Bottom panel shows source locations of dissolved organic carbon (DOC) and dissolved inorganic carbon (DIC) to the hyporheic zone (HZ). Top panel redrawn and modified with permission from Roy Haggerty. Bottom panel summarized from Corson-Rikert et al., (2016). Note: We investigated the metabolism of organic C – DOCst and POCb – along short-time scale near-stream hyporheic flow paths (red). The mesocosms were designed to eliminate potential confounding factors of groundwater (blue) or shallow hillslope water inputs (brown) as well as vertical exchanges with the overlying riparian soil (green). For simple organic C molecule, the stoichiometry can be generalized as: $nO_2 + n(CH_2O) = nCO_2 + nH_2O$ (where n = moles, and organic molecule of structure CH_2O represent both DOC_{st} and POC_b.

2.3 Study site

This study was conducted near the mouth of a 95.6 ha second-order basin, Watershed 1 (WS1), located in the H. J. Andrews Experimental Forest, in the western Cascades of Oregon, USA (44º 12' 28.0" N, 122º 15' 30.0" W). WS1 ranges in elevation from 439 m to 1027 m, and hillslopes average 59% slope (Bernstein and Rothacher, 1959). Climate of the region is characterized as marine temperate with cool, wet winters and warm, dry summers (Rothacher et al., 1967). WS1 lies in the snow transition zone (Rothacher et al., 1967). Rainfall is the main form of precipitation; however, when snow accumulates in winter, it usually melts within few days.

Air temperature, precipitation, and stream discharge have been monitored at the site for several decades. Daily air temperatures recorded at this site from 1997 to 2019 indicate that lowest average air temperature occurs in December (μ = 1.9 °C; range: – 10.1 °C to 11.8 °C) and the highest average air temperature occurs in July (μ = 17.94 °C; range: 10.5 °C to 25.2 °C). Total annual rainfall from 1979 to 2018 ranged from 1009 mm to 3379 mm and averaged 2150 mm. Precipitation from November to March, generally, accounted for ~60% to ~80% of total annual precipitation. Average daily stream flow in the winter months from December to March ranged from ~100 L/s to ~ 1000 L/s (max peak flow = 1600 L/s on February 7, 1996). Average daily stream flow in summer months from June to September can be less than 1 L/s. For most of the summer, the lower mainstem stream channel is spatially intermittent.

Bedrock of the watershed is composed of tuffs, breccias, basalts, and andestites which, in the valley floor, are overlaid with extensive colluvial deposits (Rothacher et al.,

1967; Dyrness, 1969). Mass movements of soil and rock material have shaped stream channel and valley floor. An unconsolidated mixture of boulders, cobbles, and gravels fill unconstrained reaches where the valley floor can be as wide as ~14 m in the lower part of the basin (Wondzell, 2006).

The WS1 was 100% clear-cut from 1962 to 1966 using sky-line yarding system. Logging debris such as branches and treetops were burned to expose the mineral soil surface for reseeding Douglas-fir trees. Logging debris and other large logs spanning the stream channel were cut and sections blocking the channel were removed by hand. Hillslopes were replanted (Levno and Rothacher, 1969) and as of this writing, the upland forest is a mix of 50 – 60 year-old Douglas-fir (*Psuedotsuga menziesii*) with naturally reseeded western hemlock (*Tsuga heterophylla*), western red-cedar (*Thuja plicata*). Red alder (*Alnus rubrus*) has also established in the riparian zones following the harvest. Other hardwood species such as bigleaf maple (*Acer macrophyllum*), cottonwood (*Populus trichocarpa*), and Pacific dogwood (*Cornus nuttallii*) are also present in the riparian zone (Rothacher et al., 1967; Halpern and Franklin, 1990). The study reach where the well network is located is in an unconstrained section of the valley-floor of WS1 (Figure 2.2) with a longitudinal gradient of 0.14 m/m. The main stream channel consists of series of step-pool features (Kasahara and Wondzell, 2003). A few sections of stream channel have been scoured to bedrock, but majority of stream channel flows over cobble. Data from wells suggest that this colluvium is usually less than 2 m deep. The active channel is bounded on both sides by banks of vegetated riparian zone. Wetted

channel width contracts in the summer months, and rarely over tops the banks, even during winter peak flows.

2.3.1 Well network

The well network, established in summer of 1997, included 30 shallow riparian wells and 7 in-stream piezometers arrayed in six transects. Each transect had 1 mid-channel piezometer and 6 riparian wells (3 on each side of the channel). All wells and piezometers were constructed of schedule 40 PVC pipe (i.d. = 3.175 cm). Below ground length of PVC pipes varied from 1 m to 1.7 m. An array 0.32 cm diameter holes with an approximate density of 1 hole per cm^2, served as a screen along the bottom 50 cm of wells and bottom 5 cm of in-stream piezometers (Kasahara, 2000; Kasahara and Wondzell, 2003; Wondzell, 2006). We sampled 24 wells and 4 piezometers through the summer of 2014. Sampling occurred at monthly interval from June to August.

The existing, missing, and broken PVC pipes at the well-network site were replaced with stainless steel piezometers in September 2014. The new piezometers were usually driven into the hole from which the PVC had been removed, but in a few locations, they were installed adjacent to the original PVC pipe. Stainless steel piezometers were driven using pneumatic driver (Rhino® PD-55) and sledgehammer (Rob Pennington personal communication). The new well network included 43 steel piezometers arrayed in 7 transects (labeled: C to I) (Figure 2.2). Each steel piezometer (i.d. = 5.08 cm) is closed at the bottom with solid tip drive point and there is 10 cm of screen mesh above the solid tip. Sampling of new wells occurred, roughly at a monthly interval, from September 2014 to June 2015 and on three separate occasions in 2016.

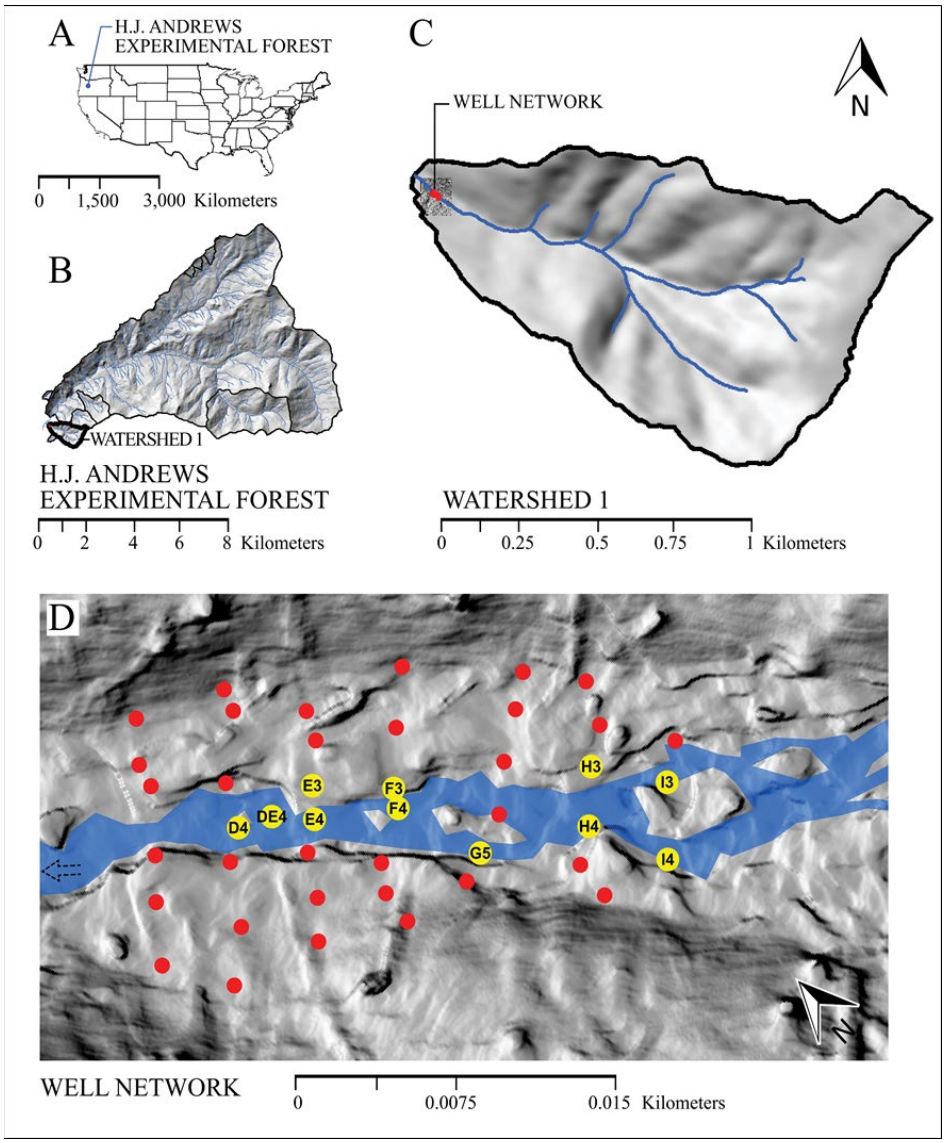

Figure 2.2 – Location of the H. J. Andrews Experimental Forest within the USA (A), location of Watershed 1 (B), and the well network (C) within the H. J. Andrews Experimental Forest. LIDAR imagery highlights features at the well network site (D). Piezometers (red) and piezometers selected for mesocosm comparison (yellow with labels) span width of the valley floor from transect C to I (uppermost transect). Dotted arrow indicates direction of the stream flow. The catchment outlines are from the H. J. Andrews experimental Forest. LIDAR imagery is from the OSU Geomatics Research Group and well survey data is from the Stream Carbon Team. Maps created in ArcGIS® and edited in Adobe® Illustrator and Indesign.

2.3.2 Hyporheic mesocosm

The hyporheic mesocosms are located on the stream bank at the WS1 gage house (Figure A.1 in Appendix A). Six 2-m hyporheic mesocosms were constructed for this project. Each mesocosm consists of two 1-m long aluminum pipe segments, each with an internal diameter of 20.3 cm and capped with HDPE end caps. Water is pumped into each mesocosm via a 0.5 cm diameter hole in the middle of each end cap. To limit the potential for non-uniform flow, to avoid large dead zones adjacent to the end cap, and to encourage laminar flow across the full cross-sectional area of the pipe segment, the inside surface of the end cap was machined with radial groves above which is a 40-µm pore-size, sintered stainless-steel mesh diffuser plate (Porous Metal Filters, Inc., 20.12 cm (7.92 inch) diameter made of sintered stainless steel with a 40 micron filter layer and with high-flow square weave support layers), which also prevented sediment from clogging the grooves (Figure 2.3).

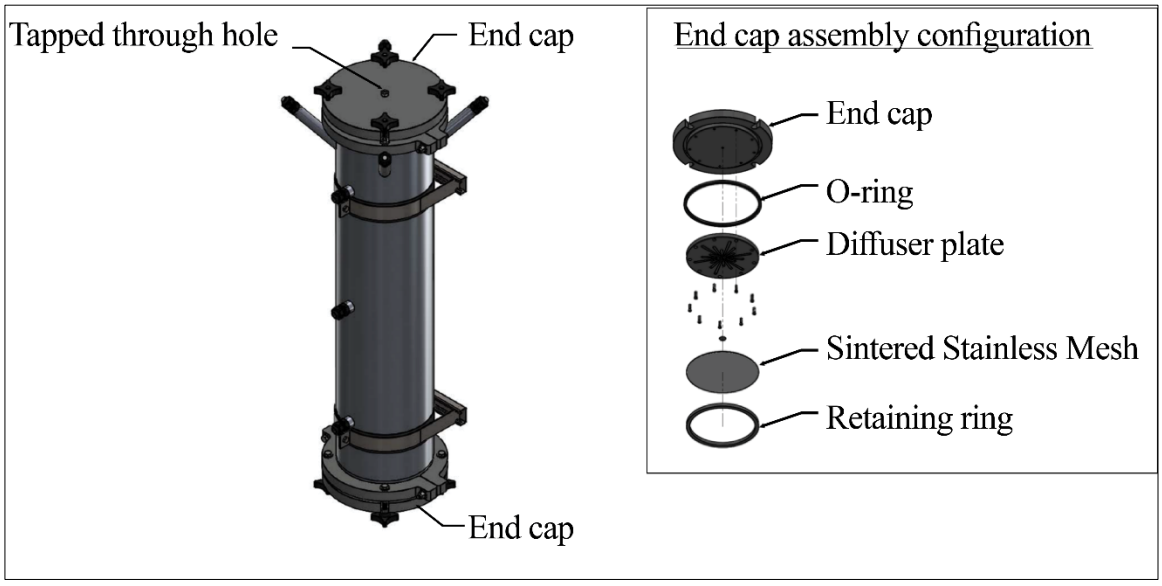

Figure 2.3 – A simplified sketch of a hyporheic mesocosm column with inset illustrating the assembly parts of an end cap. End caps are located at the top and bottom. Centrally located on an end cap is tapped through hole (bottom tapped through hole is not shown in

this figure). Drawings modified from original drawing set provided by Ben Russell, OSU to the Stream Carbon Team.

All twelve 1-m pipe segments were packed with native streambed sediment mined from the bedload accumulated in the sediment trap basin located at the mouth of the catchment, approximately 100 m downstream from the gage house. In August 2014, sediment from the trap basin was sieved through galvanized wire mesh, with square openings measuring ~6 mm (1/4 inch) on a side to remove large particulate organic matter, medium and coarse gravels, and rocks. The sieved sediment was stored in polypropylene sandbags, underwater, in the sediment trap basin until use.

Sandbags were retrieved from the pond in May 2016 and gravity drained. To ensure homogeneity during packing, two to three sandbags were emptied into a plastic tub and homogenized by mixing with a shovel. A small plastic scoop of sediment, weighing approximately 500 g, was placed in each pipe segment. This sequential packing of one scoop of sediment into each pipe segment and then continuing with another scoop, was done to spread any variation in sediment texture or organic matter content evenly across all twelve pipe segments. Once the tub was empty, the layer of sediment in each pipe was compacted using a long-handle square point tamper (10.16 cm x 10.16 cm). These steps were repeated until all twelve pipe segments were full. In total, 24 sandbags of sediment were needed to pack all 12 pipe segments.

The twelve pipe segments were mounted vertically to an aluminum frame with strut clamps. Then two pipe segments were connected via polyethylene tubing (i.d. = 0.43 cm) to construct one mesocosm. Thus, the 12 pipe-segments were connected to make six replicate, 2-m long hyporheic mesocosms (Figure 2.4 and Figure A.1 in Appendix A).

These mesocosms were enclosed in an insulated aluminum box. Field-like hyporheic temperature was maintained by continuously circulating stream water in ~18 m of soft copper tubing (3/8 in. O.D x 20 ft. Soft Copper Refrigeration Coil Tubing, Everbilt®), which was coiled to make radiators. Radiators were placed between two pipe segments because it was logistically difficult to wrap each pipe segment in copper coil. Two electric heat cables with built-in thermostat (Frost King®) were placed inside enclosures to prevent freezing in winter months.

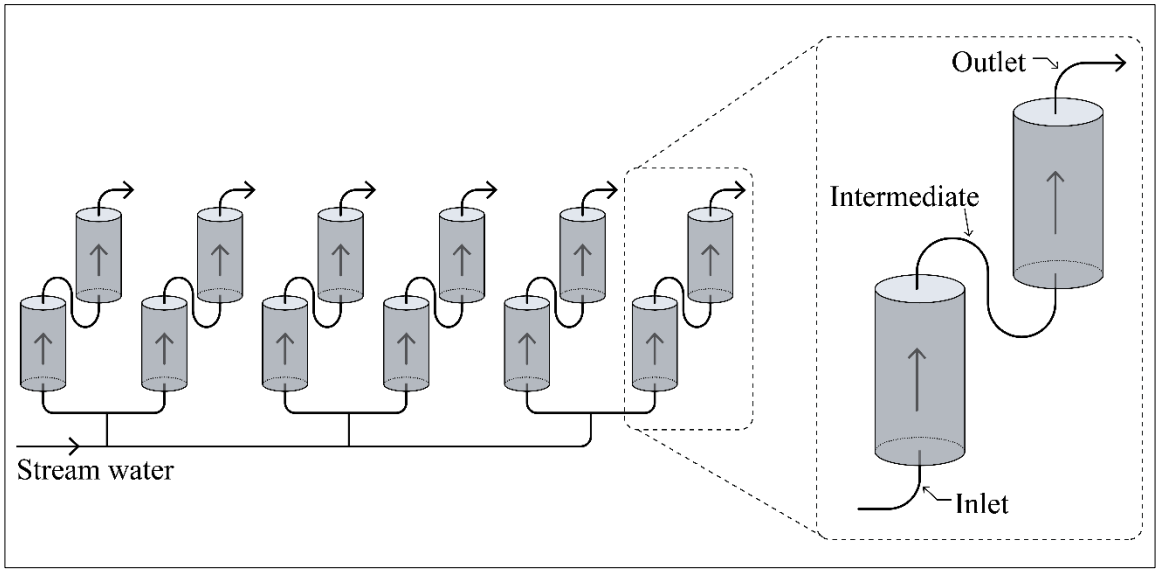

Figure 2.4 – Schematic drawing of six 2 m hyporheic mesocosms with inset illustrating location of sampling ports along 2 m hyporheic flow path.

Unfiltered stream water was pumped from the stream and through the mesocosm using a submersible pump. The water was filtered, first through a 500 µ filter, then a 150 µ filter, and then routed to two different pathways: (i) head pipe located ~3 m above the main influent line to the mesocosms, and (ii) feed line to radiator system. Water in head pipe was routed through tygon tubing to a final 50 µ filter and from there to the main feed

line to the mesocosms. Stream water has flowed through the mesocosm, continuously since May 2016, with a few notable exceptions – including short periods after large storms when filters clogged, when equipment broke down, or when power outages occurred. We monitor the flow and correct problems as soon as possible after they occur. Water sampling only occurs if flows have been maintained, uninterrupted, for at least 2 months prior to sampling.

The main feed line was split into three sub-lines, each of which was further split in two to provide influent water for each of the 6 mesocosms (Figure 2.4). Stream water flowed upwards, from the bottom orifice, through the pipe segment, and then through a diffuser plate under the top cap, and then was collected along the radial groves before exiting the top orifice (Figure 2.3). Outflow water from first pipe segment was then routed to the bottom of second pipe segment. Finally, effluent from second pipe segment was routed to central drain system, located roughly at the same elevation as the top end cap. Therefore, a flow path from influent of first pipe segment to effluent of second pipe segment was defined as a 2 m hyporheic flow path. We assumed that the tubing connecting parts of the mesocosm had minimal influence on biogeochemical processing because of limited surface area and short residence times, compared to combined length of two pipe segments.

A variety of sensors and other equipment was installed along each flow path, including in-line electrical conductivity sensors (CS547A-L, Campbell Scientific®), venturi mixers (A2Z Ozone Venturi Injector, 1/4-Inch), injection ports, and sampling ports. Electronic flow meter sensors were installed at the outlets to monitor flow rates in

real time. A high precision Hoke® valve (Part number 1335M4Y; Milli-mite 1300 Series Valve with a globe flow pattern, in stainless steel, with ¼-inch NPT male connections on both inlet and outlet, a 1-degree stem and 0.047-inch orifice with Cv = 0.01) at the distal end of mesocosm outlet was installed to control flow through each mesocosm (Figure 2.5), which was maintained as close to 48 mL/minute as was possible. Note that, at 48 mL/minute, the flow rate through the mesocosms was approximately 20 cm/hr, which was similar to the flow rates observed in the well network during tracer tests.

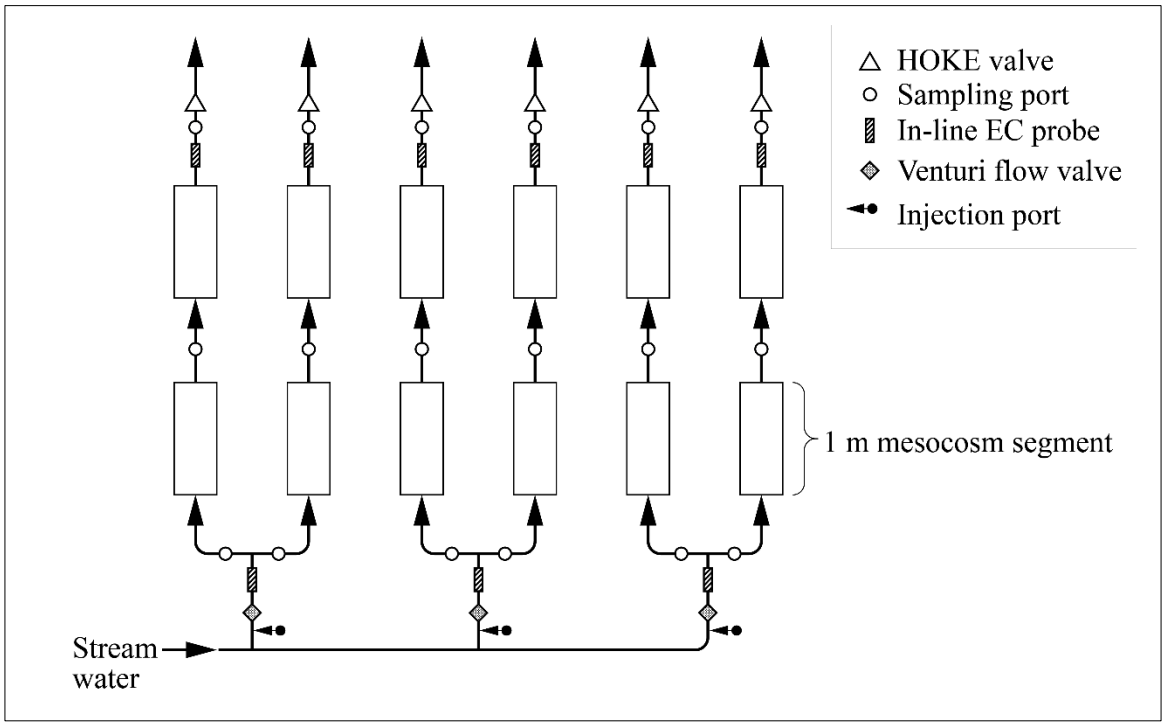

Figure 2.5 – Schematic diagram of instrumentation and sampling ports along six 2 m hyporheic flow paths.

2.4 Methods

2.4.1 Field Sampling

Field sampling was conducted from July 2014 to August 2018 over a wide range of discharge conditions. Well network was sampled fourteen times and the hyporheic mesocosm was sampled seven times (Figure 2.6).

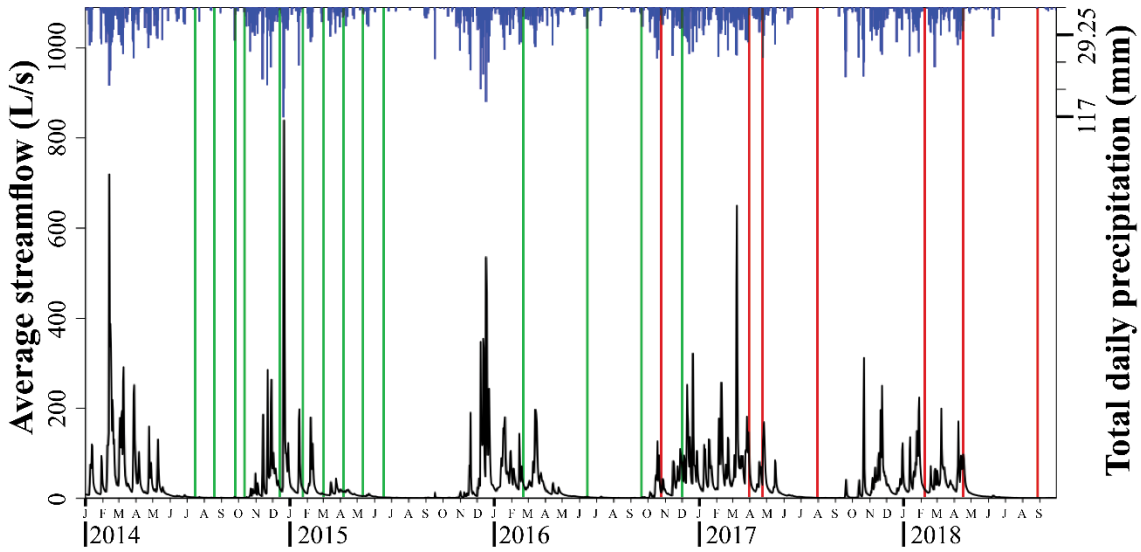

Figure 2.6 – Stream discharge and precipitation conditions over study period for well network sampling dates (green bars) and mesocosm sampling dates (red bars).

2.4.1.1 Well network

Sampling the well network took two days. Water in the piezometers was purged on the first day and samples for laboratory analysis were collected on the second day. Prior to purging, water elevation, pH, temperature, dissolved O_2, and electrical conductivity (EC) were measured. Water elevation was recorded either with a tape measure marked with a wet erase marker or with an electronic sonde. The pH was measured with a YSI Model 60 pH meter, temperature and dissolved O_2 were measured with a YSI ProODO, and EC was measured with a WTW ProfiLine Cond 3110. Once these measurements

were complete, a syringe connected to an acid-washed 2-m long length of polyethylene tubing (o.d. 0.6 cm) was used to purge approximately 700 ml of water from each piezometer, equivalent to ~35 cm of water in the piezometer.

An acid-washed 60 ml BD® syringe fitted with 3-way Luer® lock stop valves, 2 m of acid-washed tubing, and DI-rinsed ash-free GF/F filter paper held in a field-filter apparatus was used to collect samples. First, approximately 60 ml of sample water in two aliquots, ~30 ml each, was used to rinse the sample syringe and sample tubing twice. Then another 60 ml aliquot of sample water was used to rinse the field-filter apparatus and GF/F filter and pumped through the rinsed filter to rinse an acid-washed 250 ml HDPE Nalgene® bottle two times. Only then was filtered water collected. The bottle was capped after slight convex meniscus developed at its mouth to prevent air bubbles in the bottle. Lastly, 60 ml of unfiltered water was collected in the syringe and the 3-way Luer® lock stop valve was tightly closed to isolate the water sample from the air. Newly acid-washed syringes, sample bottles, stop valves, and GF/F filter papers were used for each successive piezometer, but the field-filter apparatus and the sample tubing were reused after rinsing with hyporheic water from the next piezometer. Filtered and unfiltered stream water was also collected using the same sampling technique. All water samples, including both the 60 ml syringes and 250 ml bottles, were stored in an ice chest, kept cold with ice packs, and then transported to the lab where they were put in a refrigerator (4 ºC) until analysis.

2.4.1.2 Hyporheic mesocosm

The mesocosm was sampled through ports located at the inlet, mid-point, and outlet so that water samples represented 0.0, 1.0, and 2.0-m long flow paths through the sediment. To collect a sample, flow downstream of the sample port was stopped by closing a valve, and the sample port was opened so that sample collection rate was close to 48 ml/min – the same rate as the flow through the mesocosm to minimize the potential to develop preferential flow paths through the sediment when sampling. To measure dissolved O_2 and temperature a flow-through cell (volume = ~15 ml) containing a YSI ProODO was connected to the sampling port. Next, ~20 ml water was collected in graduated cylinder to measure pH and EC. An acid-washed 60 ml BD® syringe was then attached to the sampling port to collect a water sample by manually pulling on the plunger. Two full syringe volumes, (~120 ml of sample water), was used to rinse the syringe, filter apparatus, and ash-free GF/F filter twice. Another ~60 ml of sample water, in two aliquots, was then pushed through GF/F filter apparatus and used to rinse an acid-washed 250 ml HDPE Nalgene® bottle two times. We collected 250 ml of filtered water in the HDPE Nalgene® bottle and 60 ml unfiltered water in sample syringe fitted with air-tight 3-way Luer® lock stop valve. We sampled all six inlet ports, then the intermediate ports, and finally the outlet ports. Sampling was relatively time consuming, requiring some 0.5 to 1 hour to sample each location. This was slightly faster than the travel time through each pipe segment which was approximately 5 hours.

Starting on February 6, 2018, we intentionally timed rounds of sampling to coincide with the travel time of water flowing through the mesocosm – waiting 5 to 6

hours to sample the intermediate ports and another 5 to 6 hours to sample the outlets. We also collected two stream samples, one before and one after collecting all the mesocosm samples so that changes in stream chemistry during the mesocosm sampling could be quantified. Three field duplicates were also collected during sampling.

We made a slight modification to sampling method on and after February 2018. We designed a sampling system that consisted of three sets of six acid-washed sample bottles (500 ml HDPE Nalgene®). Each set of bottles was used to collect water from the six inlet, intermediate, and outlet ports. A set of six sample bottles would be connected to six sampling ports to collect ~ 500 ml unfiltered water, regulating the flow rate to ~48 ml/min using the valve on the sample port. The water sample was collected as described above, but the syringe was connected to the outlet tube of the 500 mL bottle rather than directly to the mesocosm's sampling port (Figure 2.7). Immediately before collecting water samples using the new method, we collected a round of samples using the previously described syringe method. We then tested for difference between the sampling methods using paired two sample t tests on DOC concentrations at the inlet, intermediate, and outlet sampling ports. Our results indicated that the modification of the sampling technique did not influence the measured DOC concentration (Tables B.1 – B.3 in Appendix B).

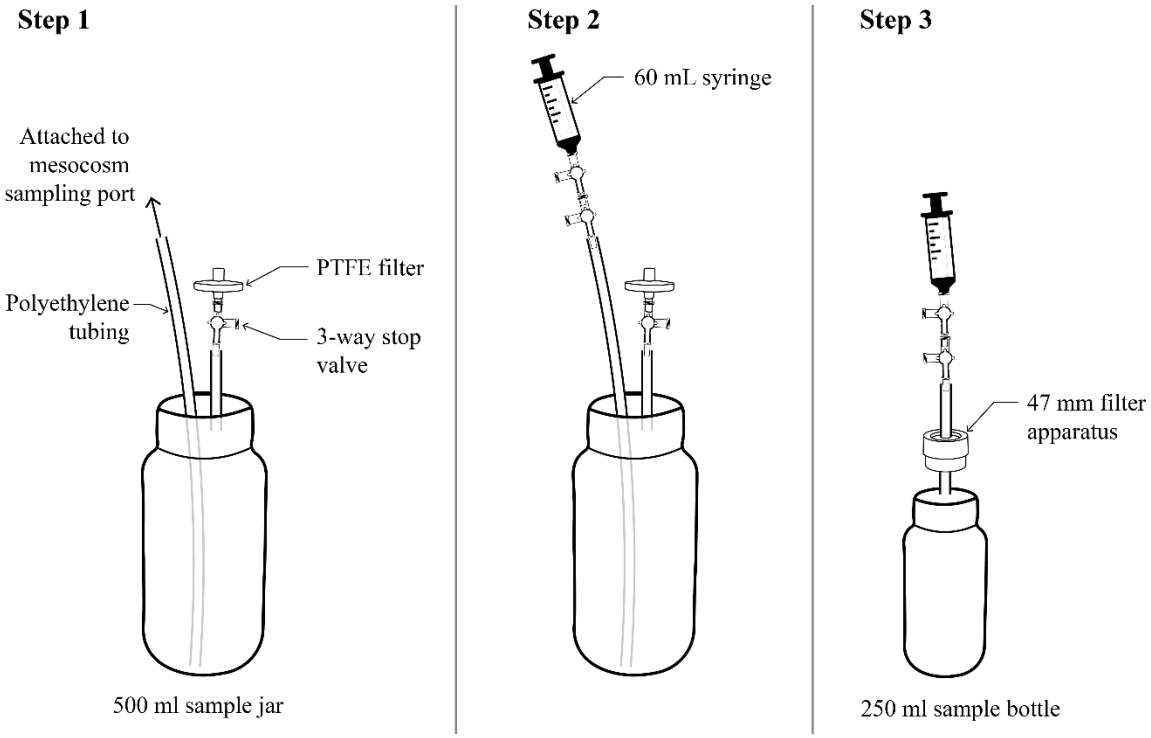

Figure 2.7 – Schematic of sample jar collection setup. Steps 1 to 3 repeated as needed to fill 250 ml sample bottle.

2.4.2 Laboratory procedure

All laboratory work was completed at the Institute for Water and Watersheds Cooperative Chemical Analytical Laboratory (CCAL) in Corvallis, Oregon. Prior to field work, all laboratory and field sampling equipment, including 250 ml HDPE bottles, 40 mL borosilicate vials (VWR TraceClean), 60 mL syringes with Luer-Lok® tips, Cole-Parmer® masterflex fitting polycarbonate stopcocks with Luer® connections (item# SK-30600-03), Advantec® Polypropylene Filter Holder for 47-mm filter (item# UX-06623-22), and sample tubing (o.d. 0.635 cm) were rinsed in deionized water, soaked in a 10% v/v HCl acid-bath solution overnight, re-rinsed and soaked in deionized water, and air-dried in a fume hood. The borosilicate vials for DOC analysis were further processed by

combusting them in muffle furnace at 550 ºC for three hours. After they cooled, they were stored in air-tight containers. The 47 mm GF/F glass microfiber filters were rinsed in 1 L of deionized water and dried overnight in a drying oven 70 ºC – 80 ºC. Each filter paper was then was placed in aluminum foil packet (~5 cm by ~5 cm) and combusted in a muffle furnace at 550 ºC for three hours. After cooling, the aluminum foil packets were sealed and stored in air-tight clean Ziploc® bags (CCAL, unpublished, 2013).

The CCAL standard operating procedure for DOC and DIC analyses were developed from American Public Health Association (APHA) methods. Citations for the methods used in DOC and DIC analyses will be in the following format: (CCAL standard operating procedure, APHA method, comparable EPA method, method detection limit).

Unfiltered syringe samples collected in the field were analyzed for DIC. Prior to DIC analysis, stopcocks were removed from syringes and immediately replaced with 25 mm diameter VWR® Syringe filters with polypropylene housing. Sample water in syringe were pushed through filter into an acid-washed 40 mL borosilicate vial. The vial was filled by holding it at an angle so sample water ran down its side wall. When vial was close to being full, it was straightened, filled to its brim, and capped as soon as sample formed inverted meniscus at its mouth. Filtered samples were then analyzed on a Shimadzu TOC-VSCH Combustion Carbon Analyzer within 72 hours (CCAL 21A.1, n/a, n/a, 0.05 mg C/L).

Field filtered water samples in 250 mL Nalgene® bottles were analyzed for DOC. An aliquot (~25 mL) of field-filtered 250 mL sample was analyzed for DOC. Aliquots were poured into baked 40 mL borosilicate vials and analyzed on a Shimadzu TOC-

VSCH Combustion Carbon Analyzer (CCAL 20A.3, APHA 5310B, EPA 415.1, 0.05 mg C/L).

2.4.3 Median travel times - hyporheic mesocosm

We conducted five NaCl tracer injection experiments in the mesocosm over the duration of this study (Table 2.1) and used continuous measurements of EC measured at the inlet and outlet locations to calculate median travel times of stream water through mesocosm. In each experiment, a conservative tracer solution (NaCl) was injected into two of the three sub lines serving as source water for a pair of mesocosms (Figure 2.5). The injectate was pumped into the mesocosm at a rate of 2 to 3 ml/min using two HPLC pumps (Series I P-040 Metering HPLC Pump, Scientific Systems®). Each injection experiment lasted for approximately 100 hours and ECs (µS/cm) were recorded at 5 minutes interval with in-line CS547A-L.

Table 2.1 - Dates and durations of five mesocosm injection experiments.

Injection Experiment	Date	Duration of injection (hrs)
1	10/23/2016 – 10/27/2016	~97
2	04/23/2017 – 04/27/2017	~97
3	07/29/2017 – 08/02/2017	~97
4	04/17/2018 – 04/21/2018	~107
5	08/28/2018 – 09/02/2018	~111

The pumping rate was close to the lower limit of the HPLC pumps and this likely caused the sharp fluctuations in EC observed in the inlet EC meters and slight variations in the pumping rates likely lead to the observed variability in plateau tracer concentrations (Figure 2.8 and Figures A.2 – A.5 in Appendix A). Due to this variation, I

averaged the background EC over 20 – 25 hours and the plateau EC over 20-25 hours. I calculated the median travel time of stream water through a mesocosm using (Eq. 1).

$$EC_{MTT} = \frac{(EC_P - EC_B)}{2} \quad \text{(Eq. 1)}$$

where, EC_B is the averaged background EC and EC_P is the averaged plateau EC.

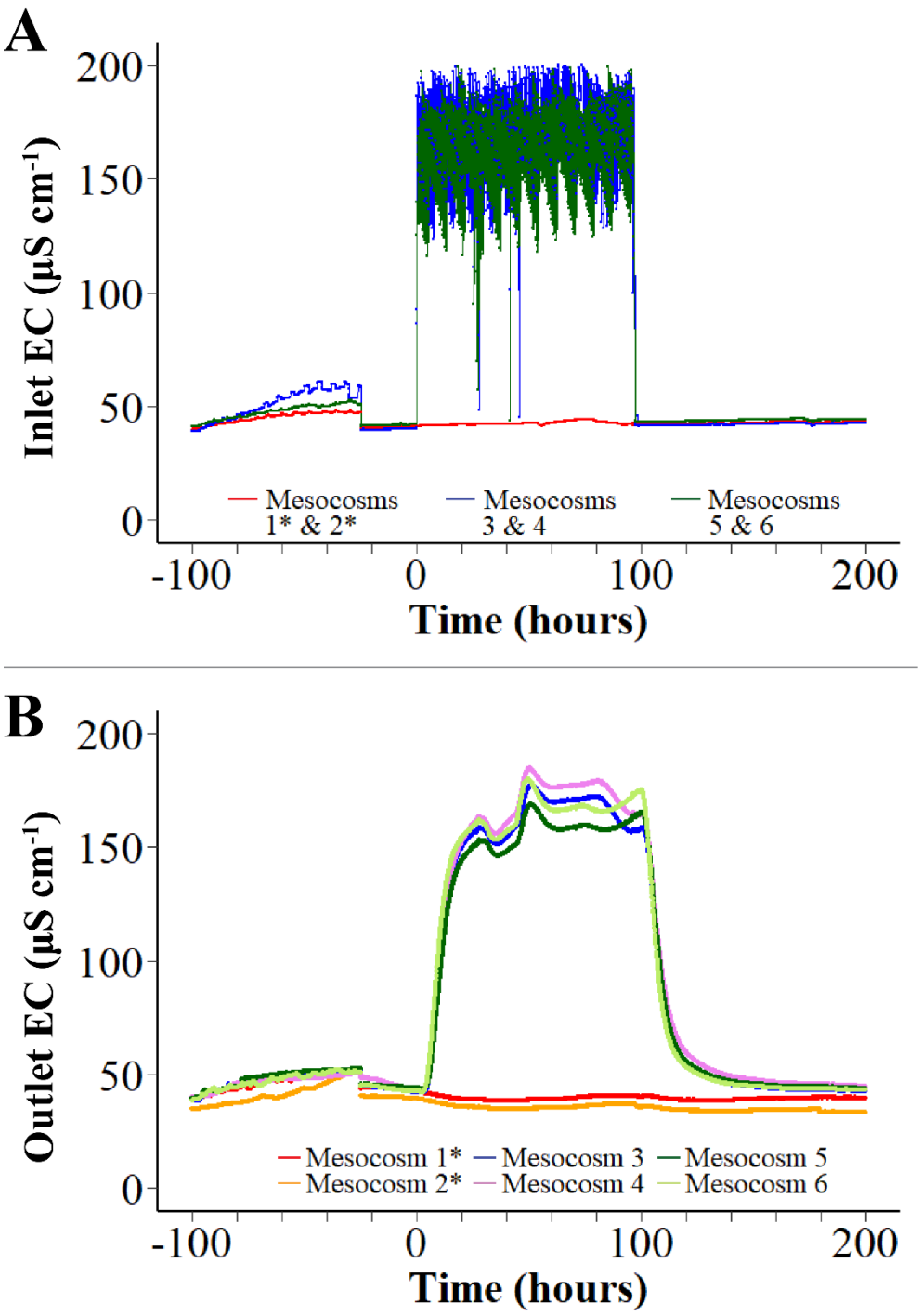

Figure 2.8 – Breakthrough curves of electrical conductivity measured at the inlet (A) and the outlet (B) from1st NaCl tracer injection experiment conducted from 10/23/2016 to 10/27/2016. Mesocosms with * are control mesocosms that did not receive tracer treatments.

The median residence time was then calculated as the time, from the beginning of the injection, required to attain EC_{MTT}. Only 4 of the 6 mesocosms received tracer injections in any given experiment. Thus, on sample dates when tracer experiments were not conducted on a given mesocosm, the mesocosm was assigned a median residence time equal to the average of the travel times calculated from all tracer injection experiments conducted on that mesocosm.

2.4.4 Selection of a subset of piezometers from the well network to compare with mesocosm

We selected a subset of piezometers with travel times similar to the mesocosm and dominated by stream source water to compare our mesocosm results to the actual HZ. The investigation conducted by Pennington (2019) at this same site provided us with the median travel times of stream water to each piezometer. Others have also conducted NaCl tracer tests at this well network site and used EC as a surrogate for Cl^- concentrations to characterize breakthrough curves of Cl^- (Wondzell, 2006; Gonzalez-Pinzon et al., 2014; Ward et al., 2016 However, Pennington's (2019) travel time estimates are the most relevant to our study because the earlier studies were conducted using the PVC wells where as most of our water samples were collected from the stainless steel piezometers installed in September 2014.

Pennington (2019) conducted tracer tests at the well network site from 2014 to 2016 under a wide range of discharge conditions. An array of *in situ* EC/temperature sensors (Campbell 547A) within the stream and piezometers continuously measured EC at a 10-minute intervals which was used to estimate travel times of stream water to each

piezometer along hyporheic flow paths. Median travel time of stream water to each piezometer were calculated using transfer function analysis and the zeroth moment ratio was also calculated for each piezometer to estimate the proportion of stream water at each piezometer (Appendix B in Pennington, 2019). Using Pennington (2019) results, we then averaged the zeroth moment ratios of all tracer tests for each piezometer and only piezometers with the averaged zeroth moment ratio close to 1 and median travel times ≤ 24 hours were used to compare with the mesocosm.

2.4.5 Calculations

To compare utilization of O_2, metabolism of DOC, and accumulation of DIC along gradients of hyporheic flow paths in the mesocosm, the concentrations of O_2 (mg O_2/L) recorded on site and DOC (mg C/L) and DIC (mg C/L) from laboratory analyses were converted to molar units using (Eq. 2). For X = DOC or DIC, molecular weight of 12.0107 g/mole (molecular weight of C) is used in the denominator. Molecular weight of 31.99 g/mole (molecular weight of O_2) is used for X = O_2.

$$X\left(\frac{\text{mg}}{\text{L}}\right) * \frac{1\text{g}}{1000\text{mg}} * \frac{1}{\text{Molecularweight}\left(\frac{\text{g}}{\text{mol}}\right)} * \frac{1000\text{millimole}}{1\text{mole}} = X(\text{mM}) \qquad \text{(Eq. 2)}$$

We then calculated ΔO_2, ΔDOC_{st}, and ΔDIC as the difference between concentrations measured at the outlet minus those at the inlets. Thus, the positive Δ values indicate production and negative Δ values indicate consumption. The ΔO_2, ΔDOC_{st}, and ΔDIC were calculated for all six mesocosms for each of the seven sampling dates and the 6 values were from the mesocosm were averaged on each sampling date. We assumed that respiration is the only process that utilized O_2 and produced DIC along the hyporheic flow paths through the mesocosms, thus ignoring other processes such as

chemical weathering metal oxidation, and other biogeochemical reactions that could influence ΔO_2 and ΔDIC. Given this assumption, we can examine if the observed loss of DOC_{st} could explain the observed loss O_2 and gain of DIC. We assumed a 1:1 stoichiometric relationship for carbon metabolism, i.e., that 1 mole of DOC_{st} accounts for consumption of 1 mole of O_2 (Findlay et al., 1993; Findlay and Sobczak, 1996; Battin et al., 2003; Mermillod-Blondin et al., 2005) and production of 1 mole of DIC.

The consumption of O_2 and production of DIC were modeled as first-order kinetic reactions with O_2 consumption rate coefficient (k_{O_2}) and DIC production rate coefficient (k_{DIC}) obtained from the slope of the natural log of O_2 or DIC regressed against median travel time. For instance, uptake rate of O_2 can be modeled as first order exponential decay as (Eq. 3).

$$[O_2]_t = [O_2]_o * e^{-k_{O_2} t} \quad \text{(Eq. 3)}$$

where $[O_2]_t$ is measured concentration of dissolved oxygen at median travel time (t), $[O_2]_o$ is concentration of dissolved oxygen at inlets and k_{O_2} is the rate constant. This equation can be linearized by taking the natural log (Eq. 4).

$$\ln[O_2]t = \ln[O_2]o - k_{O_2} t \quad \text{(Eq. 4)}$$

Plotting $\ln[O_2]$ with respect to time for a first-order reaction gives a straight line with the slope of the line $-k_{O_2}$ which can be calculated with (Eq. 5) and the unit of k_{O_2} in a first-order reaction is $time^{-1}$.

$$k_{O_2} = -\ln \frac{[O_2]_t}{[O_2]_o} * \frac{1}{t} \quad \text{(Eq. 5)}$$

Similarly, the k_{DIC} can also be modeled as first-order exponential increase (Eq. 6) and k_{DIC} calculated using (Eq. 7).

$$[DIC]_t = [DIC]_o * e^{k_{DIC}t} \quad \text{(Eq. 6)}$$

$$k_{DIC} = \ln \frac{[DIC]_t}{[DIC]_o} * \frac{1}{t} \quad \text{(Eq. 7)}$$

2.4.6 Statistical methods

Our dataset has a mix of continuous and categorical variables with overall sample size of 42 observation (6 mesocosms x 7 dates). The continuous dependent variables are k_{O_2} and k_{DIC} and the continuous independent variables are temperature, time since packing (elapsed days), and inlet DOC concentrations. We also have season as a categorical independent variable with two levels: Summer-Fall and Winter-Spring. The mesocosms were sampled across seven sampling dates at unequal time interval. First sampling occurred at 150 days after the mesocosms were packed, second sampling occurred at 307 days, third sampling occurred at 331 days, fourth sampling occurred at 429 days, fifth sampling occurred at 621 days, sixth sampling occurred at 690 days, and seventh sampling occurred at 823 days. Here the days indicated time elapsed since the mesocosms were packed. First, fourth, and seventh sampling events were categorized as Summer-Fall and second, third, fifth, and sixth sampling events were categorized as Winter-Fall.

We used a general linear mixed effects model to account for possible autocorrelation caused by the unequal interval repeated measures in addition to the mesocosm effect. First, we ran a full model without any correlation structure and then we

re-ran the initial model with various correlation structures (random = ~time|mesocosm) such as Linear spatial, Gaussian spatial, Exponential spatial, and Spherical spatial correlation structures. We then selected the model structure with lowest Akaike Information Criterion (AIC) to examine the relationship between of temperature, season, and time since packing (elapsed days), and inlet DOC concentrations on k_{O_2} and k_{DIC}. There are 42 k_{O_2} and 42 k_{DIC} values (6 mesocosm x 7 sampling dates) in our dataset. The small sample size and study design limited these analyses to main effects of each explanatory variable on our response variables, k_{O_2} and k_{DIC}. Statistical analyses were conducted in R version 4.0.3 using 'NLME version 3.1-149'(Pinheiro et al., 2021).

2.5 Results

2.5.1 General background information and biogeochemical patterns

The well network was sampled 14 times between July 2014 to December 2016 and the mesocosm was sampled 7 times between October 2016 to August 2018. Sampling targeted baseflow or near-baseflow conditions, however, this was not always possible, especially during the winter rainy season. Daily stream discharges ranged from 0.169 to 838.5 L/s for the duration of our study whereas sample were collected at discharges ranging from 0.5 to 123.7 L/s (Table 2.2).

Table 2.2 – Hydrologic (Johnson et al., 2020) and climatic (Daly et al., 2019) conditions for each sampling date at the Watershed 1 stream gage and the PRIMET benchmark meteorological station.

Date	Avg. Air Temperature *ºC*	Avg. EC *µS/cm*	Avg. Stream Temperature *ºC*	Avg. Q *L/s*	5-day ppt total *mm*	21-day ppt total *mm*
well network sammpling						
7-15-2014	20.8	63.2	16.1	1.8	1.5	37.1
8-19-2014	20.4	60.1	15.8	0.7	2.8	5.4
9-24-2014	14.7	62.7	14.4	3.4	0.0	0.3
10-12-2014	10.8	72.4	11.3	0.9	4.3	51.7
12-14-2014	1.3	40.4	6.7	21.8	28.0	217.1
1-25-2015	6.8	40.0	8.2	18.0	0.8	117
3-1-2015	0.9	45.0	4.7	9.7	20.5	57.1
4-5-2015	3.8	43.4	6.6	14.8	30.4	124.6
5-10-2015	13.6	50.8	10.1	4.7	2.0	27.9
6-16-2015	17.5	58.0	13.6	1.8	0.0	8.3
2-21-2016	2.9	37.9	6.6	36.9	52.8	162.2
6-14-2016	7.8	50.3	10.9	4.0	11.7	12.8
9-19-2016	12.7	66.4	13.0	0.8	10.3	23.9
12-1-2016	3.5	40.4	8.0	78.8	78.1	243.6
hyporheic mesocosm sampling						
10-23-2016	8.9	43.5	9.9	23.1	76.3	307.6
03-29-2017	7.8	35.0	7.8	123.7	91.6	292.1
04-22-2017	9.4	39.6	8.4	38.1	60.3	140.0
07-29-2017	18.8	56.5	15.0	0.9	0.0	0.0
02-06-2018	4.0	43.2	7.1	22.1	10.7	228.2
04-16-2018	3.6	39.1	6.8	70.4	80.5	205.0
08-27-2018	16.1	71.4	14.3	0.5	0.2	0.2

2.5.1.1 Well network

Temperature of hyporheic water among all piezometers on each sample date remained relatively constant regardless of travel time. These temperatures did change seasonally so that summer and fall samples had higher water temperature than winter and spring samples. Hyporheic water temperatures reflected local stream water temperature on each sample date. Concentrations of O_2 declined with increased in travel time and

decreased more on warmer sampling dates than colder sampling dates. Concentrations of DOC in the HZ remained relatively unchanged, neither increasing nor decreasing substantially with increased travel time. The highest concentrations of DOC, both in stream water and hyporheic water, were observed on September 2014 (before the new stainless steel wells were installed). Concentrations of DIC in hyporheic water increased with increased in travel time (Figure 2.9).

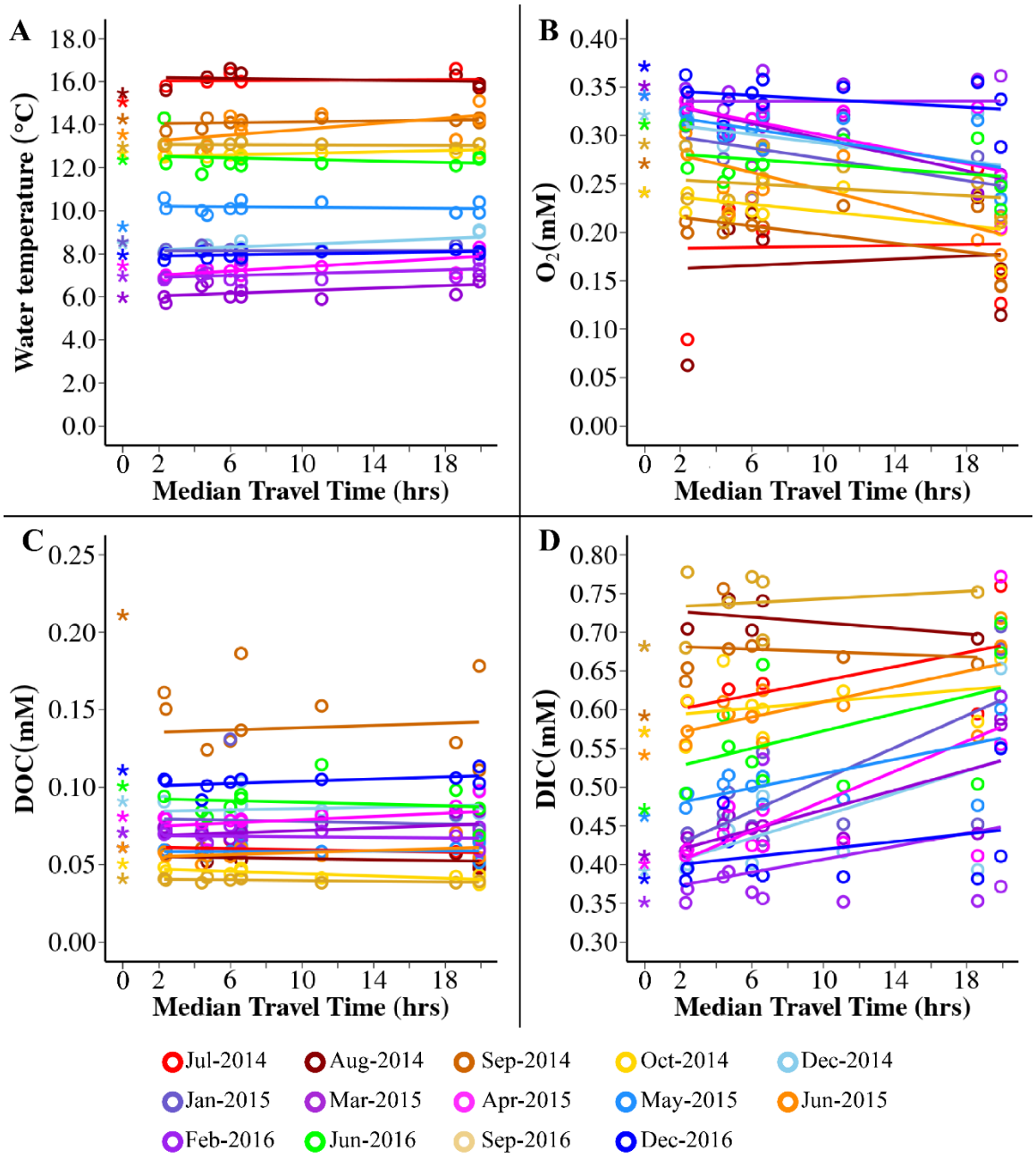

Figure 2.9 – Patterns of water temperature (A), dissolved oxygen (B), dissolved organic carbon (C), and dissolved inorganic carbon (D) for wells with range of median travel times similar to median travel times in the hyporheic mesocosms. The symbol "*" indicates stream measurement, and "o" indicate well measurements. Lines are simple linear regression lines.

2.5.1.2 Hyporheic mesocosms

Water temperatures along the 2-m flow paths through each of the six mesocosms remained relatively unchanged from inlets to outlets for the colder sampling dates, but temperature increased by as much as 5 ºC, from inlets to outlets during the warmer sampling dates. The O_2 at inlets ranged from 0.29 mM to 0.39 mM and showed seasonal trends with low concentrations on warmer sampling dates of Summer-Fall and high concentrations on cooler sampling dates of Winter-Spring. There was a consistent decline in concentrations of O_2 across the 2-m flow paths on all seven sampling dates. Concentration of DOC at inlets ranged from 0.05 mM to 0.12 mM. The lowest values of inlet DOC were on August 2018 and July 2017 and the highest concentrations of inlet DOC were on October 2016. Unlike O_2, patterns of change in DOC were not consistent over the sampling dates. DOC declined from inlets to outlets on four sampling dates, slightly increased on one sampling date and remain unchanged on two sampling dates. The concentration of DIC at inlets ranged from 0.32 mM to 0.62 mM and showed seasonal trends with higher values in Summer-Fall and lower values in Winter-Spring. Furthermore, concentrations of DIC generally increased with nominal travel time along hyporheic flow paths (Figure 2.10).

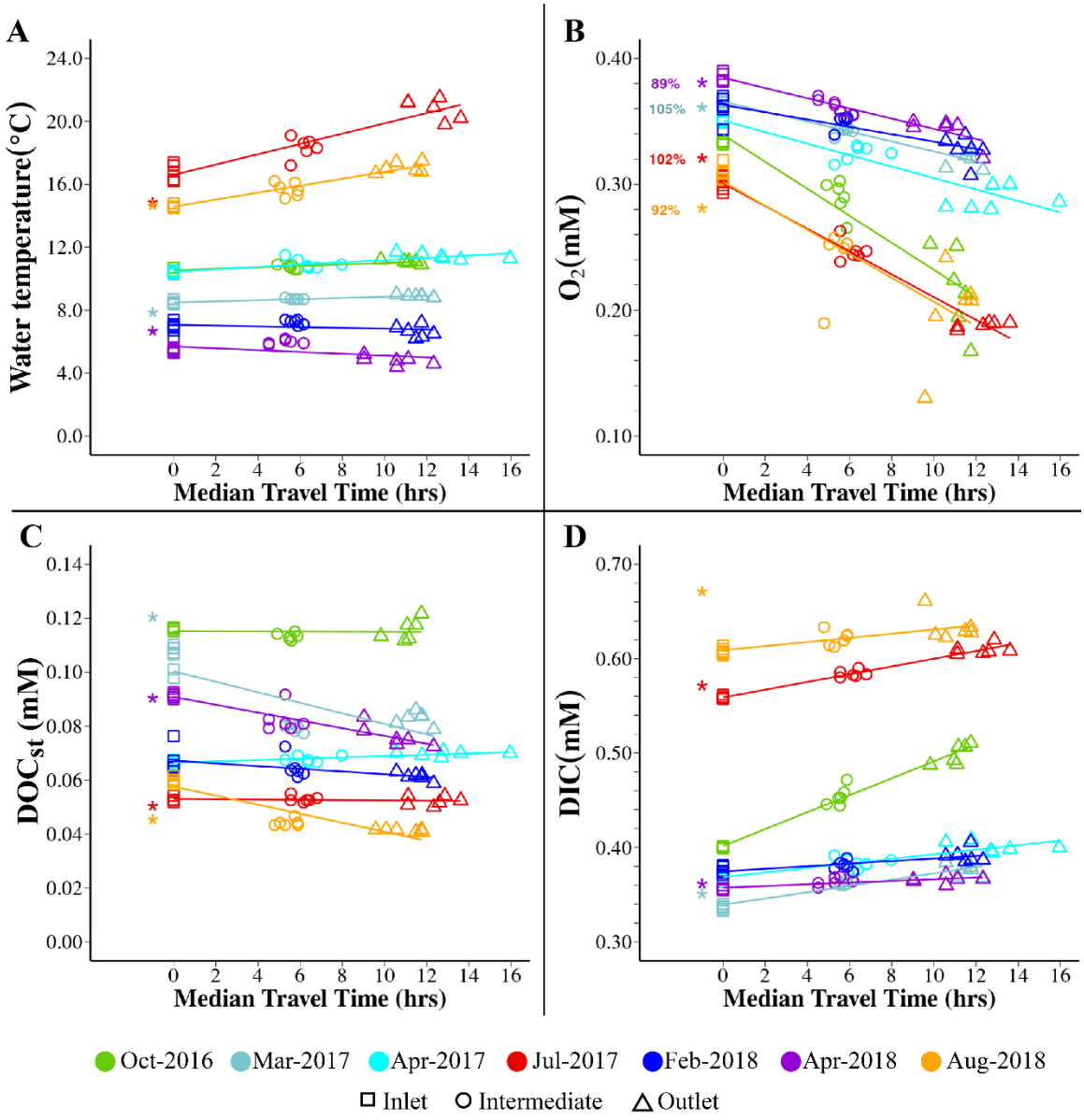

Figure 2.10 – Patterns of water temperature (A), dissolved oxygen (B), stream-source dissolved organic carbon (C) and dissolved inorganic carbon (D) across 2 m hyporheic flow paths of mesocosms. The symbol "*" indicates stream measurement. Lines are simple linear regression lines.

2.5.2 Median travel times hyporheic mesocosms from analysis of breakthrough curves

Analysis of the breakthrough curves from five injection experiments conducted in the mesocosms showed noticeable variation in median travel time among the injection experiments and among mesocosms. Median travel time ranged from 9.12 hours to 13.87 hours and averaged 10.43 hours (sd=1.06) when averaged across all mesocosms on all sample dates (Table 2.3).

Table 2.3 – Median Travel Time (MTT) of stream water through six mesocosms – M#1 to M#6 – in decimal hours. Blanks indicate no tracer injection.

Date	M#1	M#2	M#3	M#4	M#5	M#6
10/23/16			10.48	10.30	10.63	9.36
03/29/17						
04/22/17	10.68	11.12	11.22	13.87		
07/29/17	9.95	9.96			10.48	9.30
02/06/18						
04/16/18	11.00	9.12			10.48	10.10
08/27/18			9.58	10.08		
Average	10.54	10.06	10.43	11.42	10.53	9.59

2.5.3 A subset of piezometers from the well network for comparison with the mesocosm

Median travel time of stream water to the piezometers selected for comparison with the mesocosm ranged from 2.3 hours to 19.9 hours (Table 2.4) and bracketed the median travel times of stream water through hyporheic mesocosms. This subset of piezometers will be referred to as the well network from here onward.

Table 2.4 – Median travel time of stream water dominated and shorter travel time piezometers. Data courtesy of Pennington (2019).

Piezometer	Median Travel Time (hrs)	Average M0 ratio ± 1 sd
D4	2.3	0.85 ± 0.24
DE4	6.6	0.92 ± 0.11
E3	19.9	0.93 ± 0.40
E4	4.7	1.03 ± n/a
F3	6.6	0.93 ± 0.32
F4	6	1.09 ± 0.24
G5	2.4	1.07 ± 0.04
H3	19.9	2.00 ± 1.5
H4	18.6	1.60 ± 0.99
I3	11.1	1.73 ± 1.21
I4	4.4	0.72 ± 0.88

2.5.4 Patterns of ΔO_2, ΔDOC_{st}, and ΔDIC in the hyporheic mesocosms

The delta dissolved oxygen (ΔO_2) values were consistently negative, indicating consumption of O_2. The delta dissolved inorganic carbon (ΔDIC), on the other hand, were always positive indicating net production of DIC. The delta stream-source dissolved organic carbon (ΔDOC_{st}), unlike ΔO_2 and ΔDIC, did not display consistently positive or negative values. The ΔDOC_{st} values were either close to zero or slightly negative on six sampling dates, and positive on one sampling date (Figure 2.11).

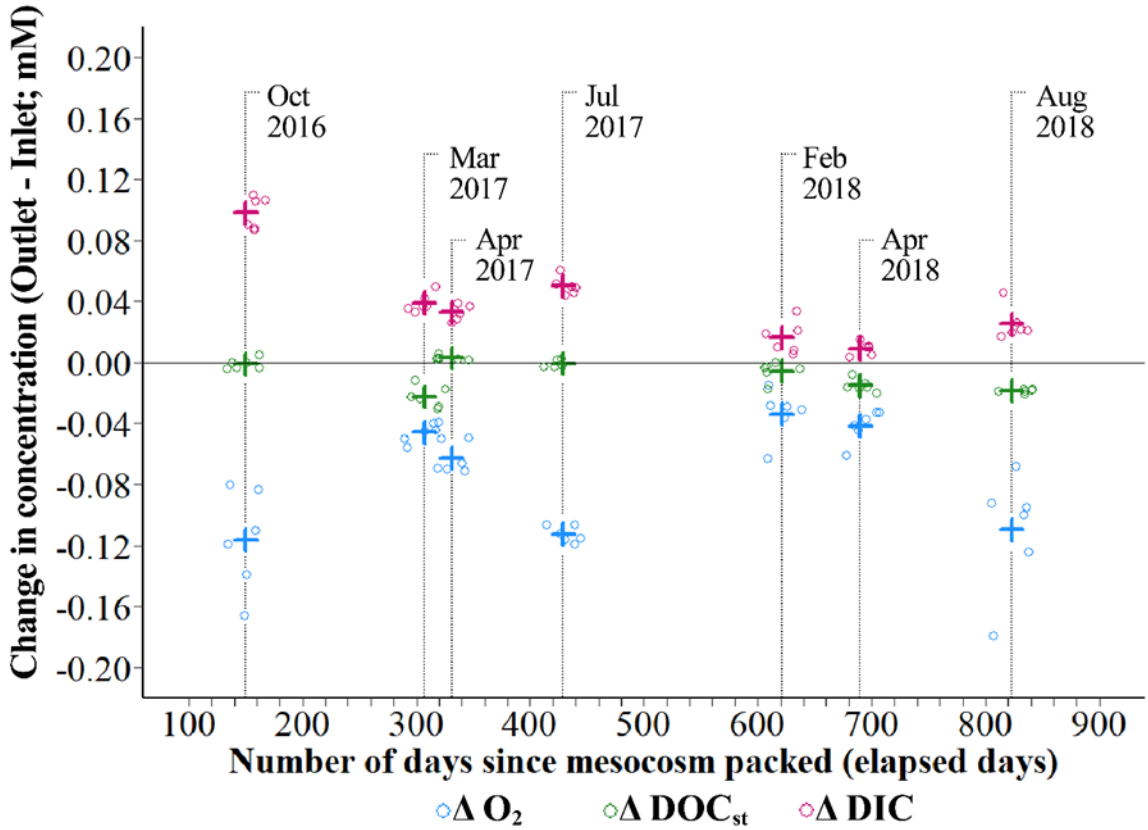

Figure 2.11 – Change in concentration of dissolved oxygen (ΔO_2), stream-source dissolved organic carbon (ΔDOC_{st}) and dissolved inorganic carbon (ΔDIC) within six hyporheic mesocosms across seven sampling dates. Positive values indicate net gain and negative values indicate net loss. The "+" symbol indicate mean of each variable for each sampling date. Note: points are jittering in the horizontal direction to display individual values without overlapping.

The ΔO_2 ranged from -0.179 mM to -0.016 mM (overall mean = -0.075 mM, sd = 0.04, overall median = -0.067 mM), the ΔDIC ranged from 0.004 mM to 0.111 mM (overall mean = 0.0388 mM, sd = 0.028, overall median = 0.0345 mM) and the ΔDOC_{st} ranged from -0.030 mM to 0.006 mM (overall mean = -0.008 mM, sd =0.010, overall median = -0.006 mM). For all sampling date, the O_2 utilized was larger than the DOC_{st} consumed and the absolute magnitudes of ΔO_2 ($|\Delta O_2|$) were at least two times greater than the absolute magnitudes of ΔDOC_{st} ($|\Delta DOC_{st}|$). The $|\Delta O_2|$ were three orders of

magnitudes greater than $|\Delta DOC_{st}|$ in two of the three Summer-Fall sampling dates, whereas the $|\Delta O_2|$ were between 2 to 19 times greater than the $|\Delta DOC_{st}|$ in the Winter-Spring. The absolute magnitudes of ΔDIC (|ΔDIC|) were also greater than the $|\Delta DOC_{st}|$ on all dates except for April 2018 (Table 2.5).

Table 2.5 – The average and confidence interval of ΔO_2, ΔDOC_{st}, and ΔDIC and the ratios between absolute ΔO_2 and ΔDOC_{st}, and absolute ΔDIC and ΔDOC_{st} over six mesocosms for each sampling date. Negative value indicates consumption and positive value indicates production. Symbol "*" indicates ΔDOC_{st} less than or close to method detection limit of 0.05 C mg/L or 0.004 mM and "§" indicates increase in DOC_{st} from inlet to outlet.

Sampling Date	ΔO_2		ΔDOC_{st}		ΔDIC		Ratio $\lvert\Delta O_2/\Delta DOC_{st}\rvert$	Ratio $\lvert\Delta DIC/\Delta DOC_{st}\rvert$
	μ	2*SE	μ	2*SE	μ	2*SE		
Oct – 2016	-0.116	0.027	-0.0004 *	0.003	0.0984	0.009	290.00	246.00
Mar – 2017	-0.0457	0.005	-0.0224	0.006	0.0388	0.005	2.04	1.73
Apr – 2017	-0.0622	0.008	0.0032 *§	0.001	0.033	0.004	19.44	10.31
Jul – 2017	-0.113	0.004	-0.0007 *	0.0017	0.0506	0.005	161.43	72.29
Feb – 2018	-0.0336	0.012	-0.0056 *	0.005	0.016	0.009	6.00	2.86
Apr – 2018	-0.0414	0.009	-0.0148	0.003	0.0094	0.004	2.80	0.64
Aug – 2018	-0.109	0.031	-0.0185	0.001	0.0253	0.009	5.89	1.37

There was strong seasonal component to magnitudes of both ΔO_2 and ΔDIC, where the magnitudes in Summer-Fall were higher than the magnitudes in Winter-Spring, but the magnitudes of ΔDOC_{st} did not display any significant seasonal differences (Figure 2.12).

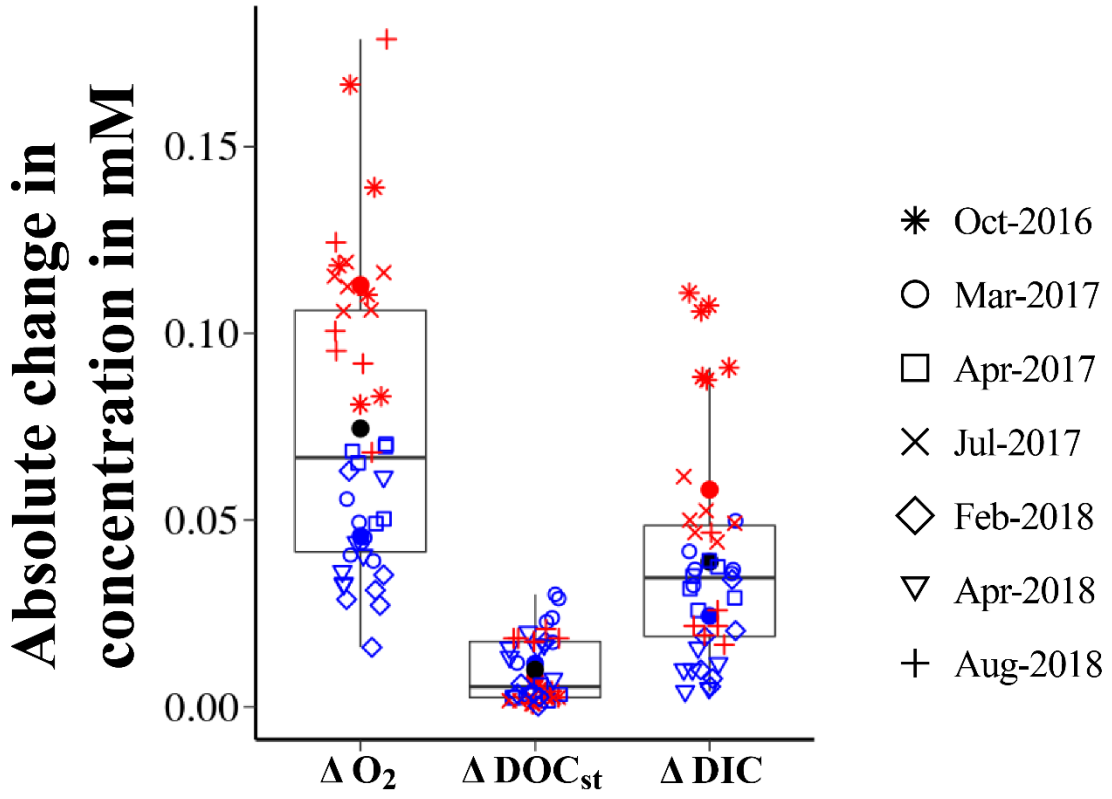

Figure 2.12 – Boxplots of absolute change in concentration of dissolved oxygen (ΔO_2), stream-source dissolved organic carbon (ΔDOC_{st}) and dissolved inorganic carbon (ΔDIC). The solid blue and red circles are seasonal averages, and the solid black circles are overall averages for each variable.

The percentage of O_2 loss that could be explained by the change in the concentration of DOC_{st} along the 2-m flow paths through the hyporheic mesocosms ranged from 0% to as high as 58% with an overall average of 18%. There was a strong seasonal difference in percentage of O_2 that could be accounted by consumption of DOC_{st}. On average, only 7% of O_2 loss could be explained by change in DOC_{st} concentration in Summer-Fall compared to 26% O_2 loss in Winter-Spring. Similarly, percent DIC produced from change in concentration of DOC_{st} also showed strong seasonal trends. On average, 48% of DIC produced in Winter-Spring could be explained

by change in concentration of DOC_{st} whereas consumption of DOC_{st} accounted for only 28% of DIC produced in Summer-Fall with an overall average of 39% of DIC explained by change in concentration of DOC_{st} (Figure 2.13).

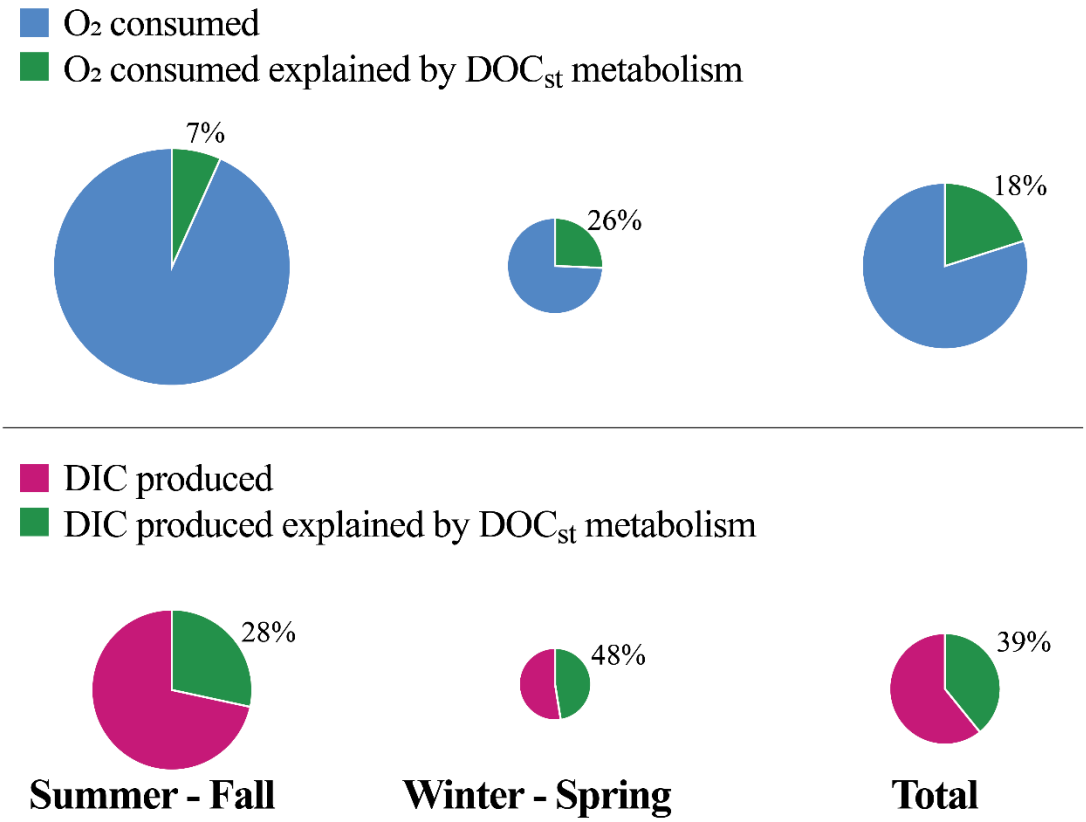

Figure 2.13 – The percentage of O_2 utilized or DIC produced that could be explained by change in concentration of DOC_{st} between inlets and outlets of the hyporheic mesocosms. Size of each "pie diagram" is proportional to the absolute magnitude of O_2 consumed (top panel) and the absolute magnitude of DIC produced (bottom panel).

2.5.5 What factors influence metabolism in hyporheic mesocosms?

We chose the model with Gaussian spatial correlation structure as our final model to examine the relationship between of temperature, season, and time since packing (elapsed days), and inlet DOC concentrations on k_{O_2}. There is evidence that

there is difference in k_{O_2} values between Summer-Fall and Winter-Spring ($F_{1,32} = 84.5$, $p = < 0.0001$, ANOVA of full model with Gaussian spatial correlation structure) and there is also a trend of increasing k_{O_2} with temperature ($F_{1,32} = 178.8$, $p < 0.001$, ANOVA of full model with Gaussian spatial correlation structure). However, when all main effects were included in the mixed-effects model with Gaussian spatial correlation structure, neither temperature ($p = 0.78$, $df = 32$) nor inlet DOC concentration ($p = 0.60$, $df = 32$) show strong relationship with k_{O_2} (Model results in Tables B.4 – B.6 in Appendix B).

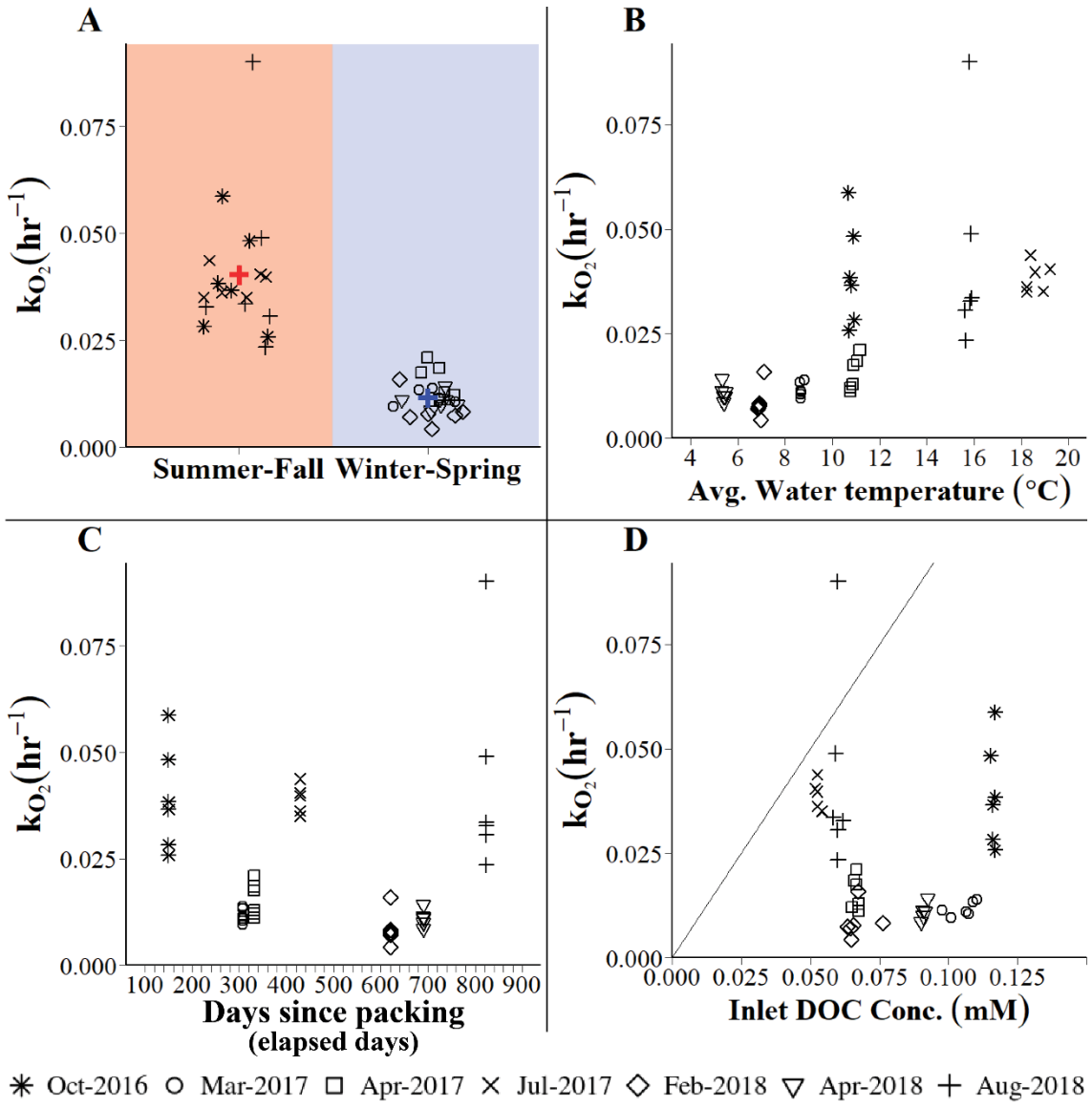

Figure 2.14 – Plots of uptake rate coefficient of dissolved oxygen (k_{O_2}) in the hyporheic mesocosm versus independent variables: (A) Season, (B) Average water temperature, (C) Elapsed days, and (D) Inlet DOC_{st} concentration. The colored "+" signs in panel A are seasonal averages of k_{O_2}. Graph "A" is shaded to indicate different seasons.

We chose the model with Linear spatial correlation structure as our final model to examine the relationship between of temperature, season, and time since packing (elapsed

days), and inlet DOC concentrations on k_{DIC}. There is evidence that there is difference in k_{DIC} values between Summer-Fall and Winter-Spring ($F_{1,32} = 2825.3$, $p = < 0.0001$, ANOVA of full model with Linear spatial correlation structure), there is also a trend of decreasing k_{DIC} with elapsed days ($F_{1,32} = 3172.5$, $p < 0.0001$, ANOVA of full model with Linear spatial correlation structure). The k_{DIC} ranged from 0.001 hr^{-1} to 0.21 hr^{-1}. It differed between seasons averaging 0.011 hr^{-1} (se = 0.0004) in the Summer-Fall and 0.005 hr^{-1} in the Winter-Spring. Unlike k_{O_2}, k_{DIC} decreased with increase in elapsed days and when all main effects were included in the mixed-effects model season, elapsed days, temperature, and inlet DOC concentrations show strong explanatory power ($p < 0.001$) (Model results in Tables B.7 – B.11 in Appendix B).

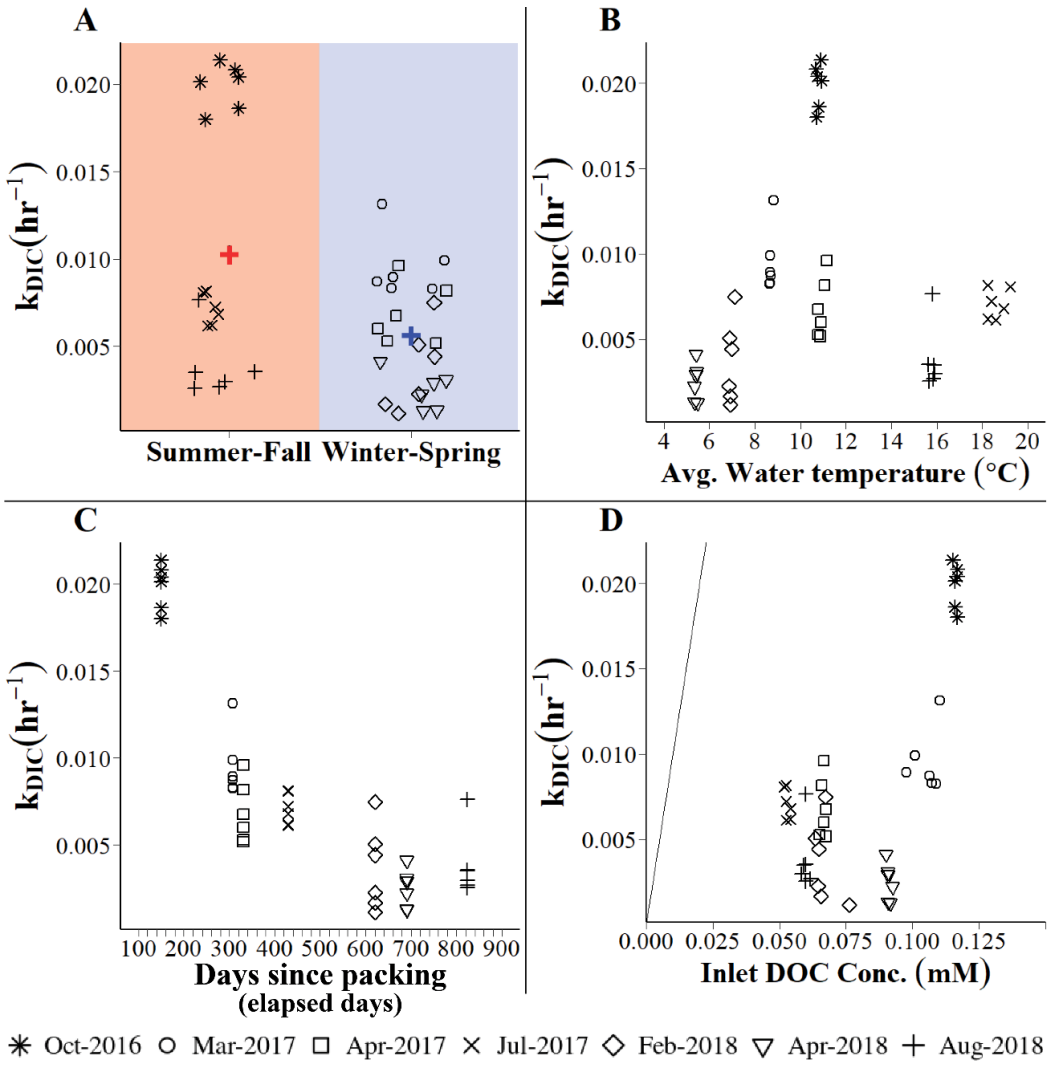

Figure 2.15 – Plots of production rate coefficient of dissolved inorganic carbon (k_{DIC}) in the hyporheic mesocosm versus independent variables: (A) Season, (B) Average water temperature, (C) Elapsed days, and (D) Inlet DOC_{st} concentration. The colored "+" signs in panel A are seasonal averages of k_{DIC}. Graph "A" is shaded to indicate different seasons.

2.5.6 How do rate coefficients from hyporheic mesocosm compare to near-stream hyporheic flow paths in the well network?

The k_{O_2} at the well network ranged from $0.1x10^{-3}$ hr^{-1} to 0.02 hr^{-1} with similar average of 0.009 hr^{-1} in both Summer-Fall and Winter-Spring (Figure 2.16). The k_{DIC} at

the well network ranged from 0.005 hr^{-1} to 0.018 hr^{-1} with Summer-Fall average of 0.009 hr^{-1} and Winter-Spring average of 0.012 hr^{-1} (Figure 2.17).

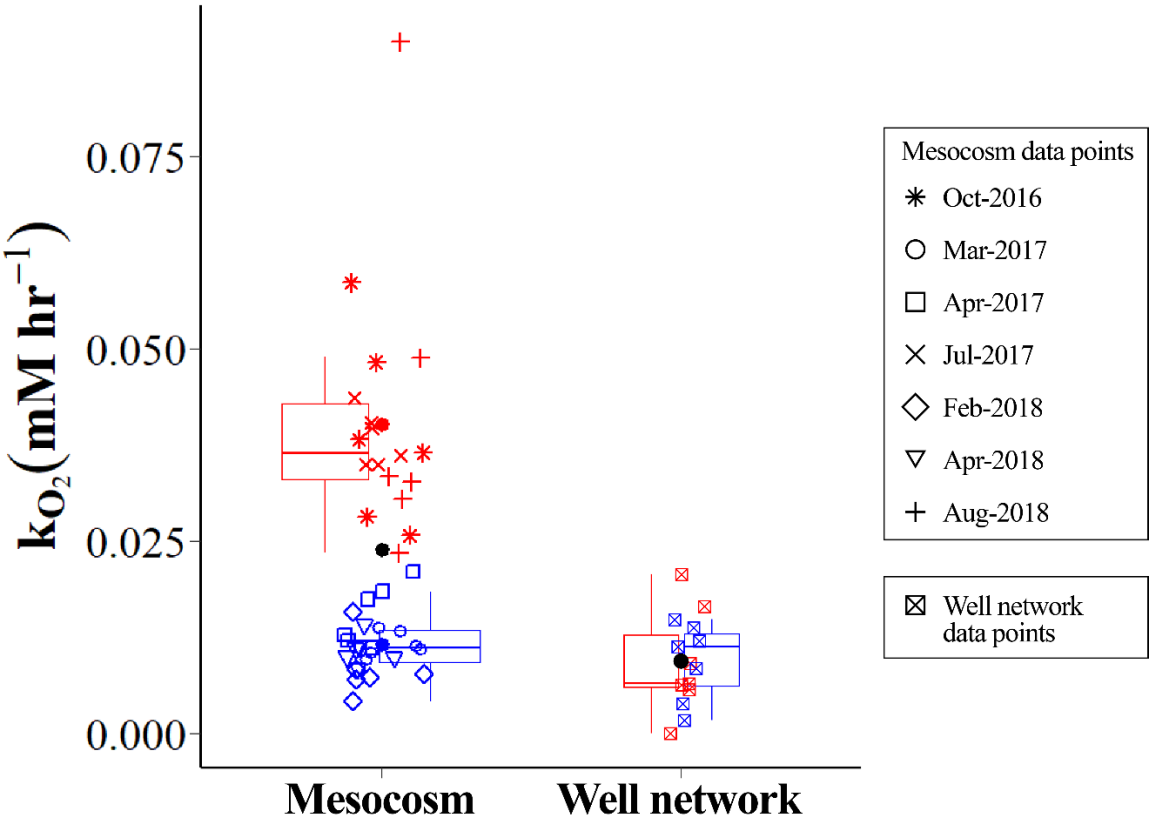

Figure 2.16 – Consumption rate coefficients of dissolved oxygen (k_{O_2}) between mesocosm and well network. Rate coefficients for Summer-Fall (red) and Winter-Spring (blue) are plotted side by side for comparison. Black circle denotes overall average for each site, whereas colored circles indicate seasonal averages for each site.

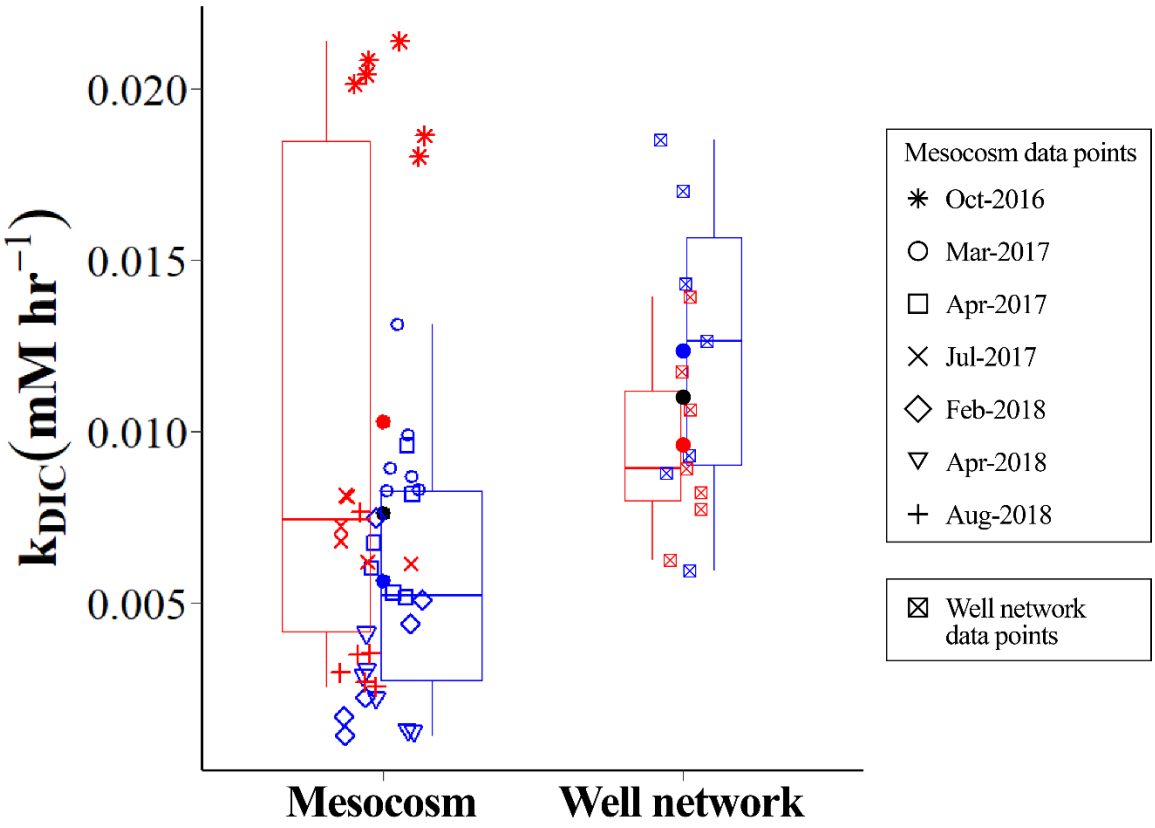

Figure 2.17 – Production rate coefficients of dissolved inorganic carbon (k_{DIC}) between mesocosm and well network. Rate coefficients for Summer-Fall (red) and Winter-Spring (blue) are plotted side by side for comparison. Black circle denotes overall average for each site, whereas colored circles indicate seasonal averages for each site.

2.6 Discussion

The HZ can play a critical role in stream C dynamics (Jones et al., 1995; Sobczak and Findlay, 2002; Clinton et al., 2010, Wagner et al., 2014; Corson-Rikert et al., 2016). Contact of stream water with metabolically active HZ sediments make environments conducive to processing of organic C (Findlay 1995). Some studies show higher rates of C processing in the HZ than in the surface stream or benthic zones (Jones et al., 1995; Sobczak and Findlay, 2002). Due to its location and lack of autotrophy, the general

assumption is that heterotrophic metabolism in the HZ is limited by bioavailable C. The supply of DOC transported via stream water has been demonstrated to make C bioavailable to hyporheic metabolism (Findlay et al., 1993; Jones et al., 1995). The role of sediment bound or buried POC in supporting heterotrophic metabolism in the HZ is often understudied because buried POC (POC_b) is often assumed to be energetically unfavorable and less bioavailabile to hyporheic metabolism. A handful of studies, to date, have compared the role of buried versus stream-source POC in fueling hyporheic metabolism (Metzler and Smock, 1990; Pusch 1996; Brugger et al., 2001; Corson-Rikert et al., 2016; Burrows et al., 2017). Our results demonstrate that POC_b can be equally important or more important than stream-source DOC in fueling heterotrophic metabolism in the HZ.

2.6.1 What is the source of metabolic C substrate for hyporheic metabolism in the hyporheic mesocosms?

Similar to other studies of C metabolism in the HZ, we measured changes in O_2, DOC_{st}, and DIC concentrations along hyporheic flow paths within our mesocosms. The changes in concentrations of DOC_{st}, O_2, and DIC are consistent among six mesocosms within a single sample date, but there are distinct seasonal patterns. The O_2 declined along flow paths with the greatest decline occurring during three Summer-Fall sampling dates. Regardless of the season the O_2 profile remained fully oxic along 2-m flow paths. The lowest O_2 measurement of 0.15 mM on August–2018 is substantially above threshold for hypoxic (0.06 mM O_2) or anoxic (0.0 mM O_2) conditions (Rounds et al.,

2006; Bodamer and Bridgeman, 2014). Under oxic conditions observed in our mesocosms, aerobic processes would predominate over anaerobic processes.

There are two possible explanations for observed decline of O_2 in our mesocosm: heterotrophy and chemolithotrophy. During chemolithotrophy, consortia of bacteria known as chemolithotropes obtain energy from the oxidation of inorganic chemicals (such as sulfide, sulfur, metal, ammonium, and nitrite) to fuel their metabolism (Jones et al., 1994). These processes are generally presumed to occur in areas where highly reduced groundwater interacts with oxic surface water in C limited environments. Jones et al. (1994) demonstrated that the O_2 loss from chemolithotrophy was as low as 1% – 3% within the oxic sediments of parafluvial zone. Our intentional engineering of mesocosms eliminate groundwater and previous studies conducted at WS1 stream have indicated low levels of nutrients and circumneutral pH in stream water. Therefore, the O_2 loss from chemolithotrophy is unlikely to influence overall O_2 decline along flow paths through our mesocosm.

Patterns of O_2 loss and concomitant increase in DIC indicate heterotrophy. There are two possible sources of organic C for heterotrophic metabolism: DOC_{st} and POC_b. The metabolism of DOC_{st} in the HZ is a function of supply and bioavailability of C (Findlay 1995; Findlay and Sobczak, 2002). Findlay et al. (1993) and Jones et al. (1995) demonstrated that DOC_{st} increased bioavailability of C to the hyporheic microbial community and fueled metabolism in the HZ where hyporheic exchange flows contained disproportionate amount of stream water. In the case of Findlay et al. (1993), DOC_{st} accounted for 18% to 68% of O_2 utilized along hyporheic flow paths on three sampling

dates. Although biological activity, indicated by the magnitude of O_2 respired, was higher in summer (July 16, 1990) than in late in late fall (August 27, 1990), the metabolism of DOC_{st}, stoichiometrically, accounted for 36% O_2 loss in summer and 68% of O_2 loss in late fall. The O_2 consumed was highest in late fall of 1991 (September 3, 1991) among three dates but only 18% of O_2 loss was attributable to the metabolism of DOC_{st} (Findlay et. al., 1993). Work by Sobczak and Findlay (2002) in the HZ of streams with differing discharge conditions, land-use type, nutrient concentrations, and stream DOC concentrations demonstrated that O_2 utilization in the HZ was a function of quality or bioavailability of C substrates. The O_2 loss between 0% and 72% was accounted by the metabolism of stream-source DOC. Brugger et al. (2001) reported DOC_{st} with about 2% to 29% bioavailable DOC could only explain up to 36% ± 25% of O_2 utilization during summer in an alpine stream.

Season can influence supply and bioavailability of C to the HZ (Findlay et al., 1993; Jones et al., 1995). In some stream systems, DOC_{st} may be more bioavailable in summer and fall (Findlay et al., 1993; Jones et al., 1995), while winter and spring may correlate to less microbially processed DOC in others (Lee and Lajtha, 2016). Hyporheic metabolism was directly correlated to surface algal production in summer in a low-order desert stream (Jones et al., 1995), where stream water downwelling in the HZ composed of highly labile or bioavailable algal exudates. In case of Findlay et al. (1993) bioavailable C in DOC_{st} was primarily made up of benthic materials in late fall which provided metabolic C substrates for hyporheic metabolism. On the other hand, the site with the lowest proportion of bioavailable DOC_{st} (e.g., the Neversink Site) displayed no

loss of O_2, whereas sites with a high proportion of bioavailable DOC_{st} displayed relative O_2 loss along gradients of hyporheic flow paths (Sobczak and Findlay, 2002).

The DOC_{st} may be highly processed or less bioavailable in alpine streams during low flow dry season (Brugger et al., 2001). For example, streams in rain-dominated watersheds typically experience low flow conditions in summer and fall. Surface flow in headwater streams can become spatially intermittent and go through several cycles of exchange with subsurface flow from the source to the mouth of the stream channel (Wondzell and Kashara, 2003). Groundwater model simulations of our study site by Kasahara and Wondzell (2003) showed that stream turnover length of 132 m at summer low flow conditions. Wondzell (2011) reported stream turnover lengths of 50 – 75 m through the HZ in WS1 and WS3 (another small headwater stream watershed located in the H. J. Andrews Experimental Forest) at late summer baseflow conditions. Such repetition of surface-subsurface exchange flows often result in accumulation of highly processed C as bioavailable fractions are stripped along hyporheic flow paths. In contrast, hydrologic events (such as rainfall, snowmelt, etc.) during late-fall, winter, and spring seasons elevate levels of humic and bioavailable DOC in stream water (Wilson et al., 2015; Lee and Lajtha, 2016).

Streamflow and DOC concentrations are often high in our stream water in winter and spring because of rain fall events (Lajtha and Jones, 2018). Lee and Lajtha (2016) reported higher proportion of bioavailable, surface, vegetation-derived DOC in stream water of WS1 during the wet season compared to the low flow dry season. This may explain the discrepancy in the metabolism of DOC_{st} between Summer-Fall and Winter-

Spring in our data. Despite the seasonal contrast in the metabolism of DOC_{st}, the molar discrepancy between DOC_{st} removed, O_2 utilized, and DIC produced strongly suggests that the heterotrophic metabolic demand in the HZ is primarily fueled by POC_b and hyporheic heterotrophy from the metabolism of POC_b is relatively greater in Summer-Fall compared to Winter-Spring, but temperature is a major factor regulating microbial activity and it is also colder in the Winter-Spring months versus Summer-Fall months.

2.6.2 Factors controlling consumption of dissolved oxygen and production of dissolved inorganic carbon in hyporheic mesocosm

Our results demonstrate that the utilization of O_2 and accumulation of DIC through microbial respiration are tightly coupled to residence time in the HZ. Studies have shown that O_2 concentrations decrease exponentially with increase in travel time (Pittroff et al., 2016; Reeder et al., 2018). Pittroff et al. (2016) used first-order kinetics model to estimate of k_{O_2} for a hyporheic flow path located in riffle-pool sequence. They reported k_{O_2} of 0.042 hr^{-1} for hyporheic flow path residence time of 0 hours to 140 hours. Reeder et al. (2018) used a high resolution sampling O_2 concentrations, over space and time, in a flume to calculate hyporheic k_{O2} using first order kinetics, and found that k_{O_2} ranged from 0.23 hr^{-1} to 120 hr^{-1} (mean = 8.2 hr^{-1}, median = 3.4 hr^{-1}). Our k_{O_2} ranging from 0.004 hr^{-1} to 0.090 hr^{-1} (mean = 0.024 hr^{-1}, sd = 0.017 hr^{-1}) are in reasonable agreement with published value of Pittroff and Gilfedder (2016) but are orders of magnitude lower than Reeder et al. (2018). This is expected because Reeder et al. (2018) stimulated O_2 uptake only when adding labile DOC substrates to their flume.

Currently, we are unaware of any studies in the HZ that report estimates of k_{DIC} from a first-order kinetic model. A study by Pett (1989) calculated accumulation rate of CO_2 from the metabolism of POC and DOC by coastal microbial communities. Under the assumption that CO_2 was produced by first-order kinetics reaction during microbial metabolism of POC and DOC, Pett (1989) reported the accumulation rate coefficients of CO_2 which ranged from 0.01 d^{-1} to 3.55 d^{-1} ($0.4x10^{-3}$ hr^{-1} to 0.148 hr^{-1}) for various moeties of POC and DOC after several days of incubation. Our k_{DIC} values range from 0.001 hr^{-1} to 0.021 hr^{-1} (mean = 0.007 hr^{-1}, sd = 0.005 hr^{-1}, median = 0.006 hr^{-1}) and are similar to the low end of the range reported by Pett (1989).

The hyporheic respiration associated with POC_b in our hyporheic mesocosm showed strong seasonal variation because the average k_{O_2} in Summer–Fall was approximately 2 times greater than the k_{O_2} during Winter–Spring. Since season is correlated with temperature in our data and temperature dependency of respiration rates are well documented in other studies (Cruz et al., 2015; Vieweg et al., 2016), we will explore relationship between temperature and k_{O_2} in detail.

Generally, an increase in temperature increases the rate of biogeochemical reactions involving O_2, organic C, and nutrients. The first-order rate constant increases exponentially with an increase in temperature (Vieweg et al., 2016) and the rate is generally expected to double for 10 ºC rise in temperature. Findlay and Sobczak (1996) investigated influence of temperature, hyporheic residence time, and concentration of stream water DOC on O_2 utilization rate and DOC removal rate within the HZ of a gravel

bar. Both temperature and residence time showed weak relationship with depletion rates of O_2 and DOC, whereas stream water DOC concentration was a strong predictor of DOC and O_2 decline (Findlay and Sobczak, 1996).

By re-graphing Findlay and Sobczak (1996) data we obtain a weak exponential relationship ($r^2 = 0.3$) between magnitudes of O_2 utilization rate and temperature (for reference Figure 4 in Findlay and Sobczak, 1996). Although their sample size (n=14) spanned from 4 ºC – 20 ºC, only 2 data points were below 10 ºC and the rest were within 10 ºC – 20 ºC which may explain the weak relationship between k_{O_2} and temperature , but the average O_2 utilization rate between 10 ºC – 20 ºC appears to be twice the average O_2 utilization rate for below 10 ºC. Although temperature did not display strong explanatory power in explaining temporal variations in k_{O_2} in our mixed effects model. The relationship between temperature and k_{O_2} show an exponential relationship ($r^2 = 0.61$) and the overall average k_{O_2} between10 ºC – 20 ºC appears to be twice of k_{O_2} for below 10 ºC. Vieweg et al. (2016) also explored relationship between O_2 consumption rate and temperature using an exponential least square fit and obtained r^2 of 0.44 and 0.64 for their two study sites.

Unlike, the relationship between k_{O_2} and temperature, the k_{DIC} and temperature relationship did not show a strong exponential trend ($r^2 = 0.06$). Perhaps this should not be surprising because accumulation of DIC and utilization of O_2 during aerobic respiration is not stoichiometrically 1:1 and the respiratory quotient, calculated as ratio of $|\Delta DIC|$ to $|\Delta O_2|$, can be lower or higher than 1 (Rodrigues and Williams, 2001). Thus,

seasonal changes in the composition of organic carbon used in HZ respiration could change the RQ and thus obscure relationships with temperature. This explanation is consistent with the observed decline in k_{DIC} over time. It is highest at the onset of sampling, October 2016, but over the course of this study, k_{DIC} declines exponentially with time. This suggest that the bioavailability of buried POC may be declining with time.

The POC, like DOC, is a mixture of organic C substrates with range of oxidation states and attached functional groups. Similar to DOC, bioavailability of POC can influence hyporheic activity (Fischer et al., 2002). Pusch (1996) demonstrated that the rate of hyporheic respiration was noticeably higher at the site with a higher proportion of POC that was loosely associated with sediment than at the site with a higher proportion of POC that were strongly associated with sediment. The trend persisted spatially (sediment depth) and temporally (season). Jones et al. (1995) showed that the HZ where organic C is primarily sourced from surface water can show slightly elevated levels of hyporheic activity following disturbance. In their case, benthic and surface organic matter that got buried in the HZ during flood events became a secondary source of organic C that supported ~15% of hyporheic metabolism, but with time respiration activity from buried organic C diminished as POC was exhausted. Pusch (1996) indicated that without the replenishment of stream water POC to the HZ, the standing stock of POC would support respiration activity for up to 4 years.

The trend observed between k_{DIC} and elapsed time (Figure 2.14 A) and relationship between respiratory quotient and elapsed time (Figure A.7 in Appendix A) indicate that

the bioavailable fractions of POC_b could be diminishing over time. The high proportion of the buried carbon that is metabolized on our earliest sampling date (October – 2016) could be due to a packing effect that either incorporates abundant relatively fresh organic material or from disturbance making pre-existing sediment bound organic carbon more available. We suspect that incorporation of "fresh" organic carbon is a less likely explanation because sediment was collected from a trap basin where it accumulated over the previous winter and was then stored for at least 20 months under water, before being used to pack the mesocosm. In either case, the bioavailable fractions of POC are declining resulting in both lower O_2 loss and lower DIC produced. Thus, the metabolism of POC_b, indicated by large O_2 decline and large DIC increase, at earliest date is analogous to POC becoming bioavailable after following burial of organic matter following spates as documented by Jones et al. (1995) but as the time wears on the bioavailable fractions diminish and the k_{DIC} declines exponentially, which aligns with exponential-type decay model (Cornut et al., 2010; Rovira and Rovira, 2010).

2.6.3 How do rate coefficients from hyporheic mesocosm compare to near-stream hyporheic flow paths at the well network?

The hyporheic mesocosms were engineered to simulate near-stream HZ found at the well network. Direct comparison of estimated values of the metabolic rate coefficients, k_{O_2} and k_{DIC}, between the mesocosms and the near stream hyporheic flow paths helped us understand the similarities and differences between O_2 and DIC dynamics observed in these two systems. We were particularly interested in how the rates varied seasonally and if the similarities or dissimilarities in the rates between these two systems

could help us constrain key parts of the conceptual model of hyporheic C dynamics developed by Corson-Rikert et al. (2016). The seasonality of k_{O_2} observed in the mesocosms was not observed at the near-stream hyporheic flow paths. On the other hand, the seasonal trends in k_{DIC} were opposite between mesocosm and the near-stream hyporheic flow paths. We will discuss the implications of similarities or dissimilarities in metabolic rate coefficients between engineered mesocosms and near-stream hyporheic flow paths at the well network.

Clearly, both bioavailability of organic C and temperature influence the utilization of O_2 in aerobic hyporheic zones. The large discrepancy in Summer-Fall k_{DIC} values between the mesocosms and the well network indicate that the proportion of bioavailable POC_b at the well network may be relatively low compared to bioavailabile POC_b in the mesocosm. Obviously, packing of sediment in the mesocosms is an external perturbation which may have stimulated bioavailability of POC_b. Certainly, the highest observed k_{DIC} occurred in October 2016 – the 1st sample period after packing the mesocosms. This likely explains high rates of O_2 utilization in the mesocosms in Summer-Fall and without these points k_{DIC} in the well network and mesocosm are similar. Natural disturbances, such as flooding followed by sediment deposition which are commonly associated with sediment turnover in the HZ, do not occur frequently in our headwater system. As a result, the bioavailable fractions of POC_b at the well network may have been declining over time and may be limiting aerobic metabolism during warmer temperature. However, one of the lowest values of Summer-Fall k_{O2} estimated in the mesocosm 0.024 hr^{-1} observed on August 2018, which is 823 days after packing of the mesocosms, overlap

with the uppermost Summer-Fall k_{DIC} estimated in the well network. This suggests that the readily bioavailable POC_b may get exhausted over time in the mesocosms and the ranges in Summer-Fall k_{DIC} values between mesocosms and well network will eventually overlap.

The overlap of Winter-Spring k_{O_2} values between the mesocosms and the well network suggests that the mechanisms driving the utilization of O_2 during high flow cool temperature wet season is very similar between these two systems. One plausible mechanism is that the metabolism of bioavailable DOC_{st} provides sufficient energy needed to meet metabolic activity when temperatures are cooler during the Winter-Spring season. The median of Winter-Spring k_{O_2} is slightly greater than the median of Summer-Fall k_{O_2} which is consistent with the hypothesized changes in DOC_{st} resulting from the amount of hyporheic processing occurring at low flow when the HZ turnover lengths are short (~ 70 m) versus during winter base flows when HZ turnover lengths are much longer (~ 250 m) (Wondzell, 2011).

Our data suggest that external sources of DIC might influence DIC accumulation at the well network during Winter-Spring. The Winter-Fall k_{DIC} values are much greater than Summer-Fall k_{DIC} values in the well network than the mesocosm, even early in the mesocosm study when we expect DOC to be relatively bioavailable. This suggests other sources of DIC may be influencing accumulation of DIC along hyporheic flow paths in the HZ. The most obvious source would be mixing of lateral inputs of higher DIC hillslope water or with longer-residence time groundwater. However, we intentionally

selected only piezometers dominated by stream-source water. Several of the winter well network samples occurred after stream discharge peaked during storms and these dates – 12/14/2014, 04/05/2015, and 01/25/2015 – had three highest k_{DIC} values, in increasing order, 0.0143 hr^{-1}, 0.017 hr^{-1}, and 0.0185 hr^{-1}, respectively.

Sources such as lateral inputs of hillslope, deep groundwater, and vertical infiltration of riparian soil water may influence DIC composition in hyporheic water in the well network during the wet season. However, Ward et al. (2016) showed that near-stream hyporheic flow paths were distinct from far-stream hyporheic flow paths near the valley wall. The near stream HZ was functionally isolated from overall hydraulic gradients along stream-hyporheic-riparian-hillslope continuum and was not influenced by lateral inputs. Other studies also indicate that hyporheic flow net changes very little across wide range of discharge conditions (Wondzell, 2006; Ward et al., 2012; Voltz et al., 2013). Given the evidence of minimal influence of lateral inputs, the only plausible source of DIC to the near-stream HZ is soil CO_2 which can be transported to the HZ by vertically infiltrating rainwater during the wet season.

2.7 Future work

The modular design of hyporheic mesocosms allows for establishing flow path lengths of 1 m to 12 m and the residence time of stream water can be controlled with precision metered valve to desired residence time. Future work can include conservative and non-conservative tracer injections to characterize biogeochemical processes that occur during aerobic-anaerobic changes, carbon labeled DOC tracer injections can be used to understand specific metabolism pathways, and concurrent sampling at the well

network and hyporheic mesocosms will help understand the relative role of stream-source DOC and POC_b in hyporheic metabolism and provide better estimation of production of DIC from the hyporheic metabolism.

2.8 Conclusions

We designed hyporheic mesocosms to simulate near-stream hyporheic flow paths located in the hyporheic zone of our well network site located in watershed 1 at the HJ Andrews Experimental Forest. Water samples were collected along flow paths through the mesocosms on several dates. Using a stoichiometric approach, we investigated utilization of O_2 and production of DIC due to hyporheic metabolism of DOC_{st} and POC_b. We then calculated estimates of rates of O_2 uptake and DIC production. Our results suggest that the metabolism of DOC_{st} is insufficient to account for concurrent decline in O_2 and increase in DIC across the length of hyporheic mesocosms. The metabolism of POC_b disproportionately fueled aerobic respiration in the hyporheic mesocosms during summer and fall and the contribution of DOC_{st} to hyporheic metabolism was seasonal. Monthly sampling at the well network allowed us to estimates rate coefficients of O_2 utilization and DIC production along near-stream hyporheic flow paths. Side-by-side comparison of the rate coefficients between hyporheic mesocosms and near-stream hyporheic flow paths at the well network indicated seasonal role of DOC_{st} and POC_b in hyporheic metabolism and presence of external sources of DIC at the well network site.

2.9 Acknowledgments

Data were provided by the H. J. Andrews Experimental Forest and Long-Term Ecological Research program, administered cooperatively by the USDA Forest Service Pacific Northwest Research Station, Oregon State University, and the Willamette National Forest. This material is based upon work supported by the National Science Foundation under Grant No. DEB-1440409. HJ Andrews datasets used for exploratory use are HF004, doi:10.6073/pasta/c85f62e9070a4ebe5e455190b4879c0c, HT004, doi:10.6073/pasta/9437d1603044f5b92189110dd8343763, MS001, doi.org:10.6073/pasta/c021a2ebf1f91adf0ba3b5e53189c84f

BIBLIOGRAPHY

Argerich, A., R. Haggerty, S. L. Johnson, S. M. Wondzell, N. Dosch, H. Corson-Rikert, L. R. Ashkenas, and R. Pennington (2016), Comprehensive multiyear carbon budget of a temperate headwater stream. Journal of Geophysical Research G: Biogeosciences, 121(**5**), 1306–1315, doi.org/10.1002/2015JG003050

Aufdenkampe, A. K., E. Mayorga, P. A. Raymond, J. M. Melack, S. C. Doney, S. R. Alin, R. E. Aalto, and K. Yoo (2011), Riverine coupling of biogeochemical cycles between land, oceans, and atmosphere. Frontiers in Ecology and the Environment, 9(**1**), 53-60, doi.org/10.1890/100014

Baker, M. A., C. N. Dahm, and H. M. Valett (1999), Acetate retention and metabolism in the hyporheic zone of a mountain stream. Limnology and Oceanography, 44(**6**), 1530–1539, doi.org/10.4319/lo.1999.44.6.1530

Baker, M. A., H. M. Valett, and C. N. Dahm (2000), Organic Carbon Supply and Metabolism in a Shallow Groundwater Ecosystem. Ecology, 81(**11**), 3133-3148, doi.org/10.2307/177406

Battin, T. J. (1999), Hydrologic flow paths control dissolved organic carbon fluxes and metabolism in an alpine stream hyporheic zone. Water Resources Research, 35(**10**), 3159-3169, doi.org/10.1029/1999WR900144

Battin, T. J., L. A. Kaplan, J. D. Newbold, and S. P. Hendricks (2003), A mixing model analysis of stream solute dynamics and the contribution of a hyporheic zone to ecosystem function. Freshwater Biology, 48(**6**), 995-1014, doi.org/10.1046/j.1365-2427.2003.01062.x

Battin, T. J., L. A. Kaplan, S. Findlay, C. S. Hopkinson, E. Marti, A. I. Packman, J. D. Newbold, and F. Sabater (2008), Biophysical controls on organic carbon fluxes in fluvial networks. Nature Geoscience, 1(**2**), 95–100, doi.org/10.1038/ngeo101

Berggren, M., J. F. Lapierre, and P. A. Del Giorgio (2012), Magnitude and regulation of bacterioplankton respiratory quotient across freshwater environmental gradients. ISME Journal, 6(**5**), 984-993, doi.org/10.1038/ismej.2011.157

Bodamer, B. L., and T. B. Bridgeman (2014), Experimental dead zones: Two designs for creating oxygen gradients in aquatic ecological studies. Limnology and Oceanography: Methods, 12(**7**), 441-454, doi.org/10.4319/lom.2014.12.441

Brugger, A., B. Wett, I. Kolar, B. Reitner, and G. J. Herndl (2001), Immobilization and bacterial utilization of dissolved organic carbon entering the riparian zone of the

alpine Enns River, Austria. Aquatic Microbial Ecology, 24(**2**), 129-142, doi.org/10.3354/ame024129

Burrows, R. M., H. Rutlidge, N. R. Bond, S. M. Eberhard, A. Auhl, Andersen, M. S., D. G. Valdez, and M. J. Kennard (2017), High rates of organic carbon processing in the hyporheic zone of intermittent streams. Scientific Reports, 7(**1**), doi.org/10.1038/s41598-017-12957-5

Butman, D., and P. A. Raymond (2011), Significant efflux of carbon dioxide from streams and rivers in the United States. Nature Geoscience, 4(**12**), 839–842, doi.org/10.1038/ngeo1294

Butman, D., S. Stackpoole, E. Stets, C. P. McDonald, D. W. Clow, and R. G. Striegl (2016), Aquatic carbon cycling in the conterminous United States and implications for terrestrial carbon accounting. Proceedings of the National Academy of Sciences of the United States of America, 113(**1**), 58–63, doi.org/10.1073/pnas.1512651112

Cardenas, M. B., and J. L. Wilson (2006), The influence of ambient groundwater discharge on exchange zones induced by current–bedform interactions. Journal of Hydrology, 331(**1-2**), 103-109, doi.org/10.1016/j.jhydrol.2006.05.012

CCAL (2013), CCAL Standard Operating Procedures, Oregon State University and United States Forest Service Cooperative Chemical Analytical Laboratory, Corvallis, Oregon. [Available at http://ccal.oregonstate.edu/sops, accessed July 2014.]

Clinton, S. M., R. T. Edwards, and S. E. Findlay (2010), Exoenzyme activities as indicators of dissolved organic matter composition in the hyporheic zone of a floodplain river. Freshwater Biology, 55(**8**), 1603-1615, doi.org/10.1111/j.1365-2427.2009.02383.x

Cole, J. J., Y. T. Prairie, N. F. Caraco, W. H. McDowell, L. J. Tranvik, R. G. Striegl, C. M. Duarte, P. Kortelainen, J. A. Downing, J. J. Middelburg, and J. Melack (2007), Plumbing the global carbon cycle: Integrating inland waters into the terrestrial carbon budget. Ecosystems, 10(**1**), 171–184, doi.org/10.1007/s10021-006-9013-8

Cornut, J., A. Elger, D. Lambrigot, P. Marmonier, and E. Chauvet (2010), Early stages of leaf decomposition are mediated by aquatic fungi in the hyporheic zone of woodland streams. Freshwater Biology, 55(**12**), 2541-2556, doi.org/10.1111/j.1365-2427.2010.02483.x

Corson-Rikert, H. A., S. M. Wondzell, R. Haggerty, and M. V. Santelmann (2016), Carbon dynamics in the hyporheic zone of a headwater mountain stream in the

Cascade Mountains, Oregon. Water Resources Research, 52(**10**), 7556–7576, doi.org/10.1002/2016WR019303

Cruz, J., S. Garrido, M. S. Pimentel, R. Rosa, A. M. P. Santos, and P. Ré (2013), Reproduction and respiration of a climate change indicator species: effect of temperature and variable food in the copepod Centropages chierchiae. Journal of plankton research, 35(**5**), 1046-1058. doi.org/10.1093/plankt/fbt057

Daly, C., Schulze, M., and McKee, W, (2019), Meteorological data from benchmark stations at the HJ Andrews Experimental Forest, 1957 to present. Long-Term Ecological Research. Forest Science Data Bank, Corvallis, OR. [Database]. Available: http://andlter.forestry.oregonstate.edu/data/abstract.aspx?dbcode=MS001. https://doi.org/10.6073/pasta/c021a2ebf1f91adf0ba3b5e53189c84f. Accessed 2021-02-09.

Downing, J. A., J. J. Cole, C. M. Duarte, J. J. Middelburg, J. M. Melack, Y. T. Prairie, P. Kortelainen, R. G. Striegl, W. H. McDowell and L. J. Tranvik (2012), Global abundance and size distribution of streams and rivers. Inland Waters, 2(**4**), 229–236, doi.org/10.5268/IW-2.4.502

Dyrness, C. T. (1969), Hydrologic properties of soils on three small watersheds in the western Cascades of Oregon. Res. Note PNW-111. Portland, OR: U.S. Department of Agriculture, Forest Service, Pacific Northwest Forest and Range Experiment Station. 17 p, https://andrewsforest.oregonstate.edu/publications/372

Findlay, S. (1995), Importance of surface-subsurface exchange in stream ecosystems: The hyporheic zone. Limnology and oceanography, 40(**1**), 159-164, doi.org/10.4319/lo.1995.40.1.0159

Findlay, S., and W. V. Sobczak (1996), Variability in removal of dissolved organic carbon in hyporheic sediments. Journal of the North American Benthological Society, 15(**1**), 35-41, doi.org/10.2307/1467431

Findlay, S., D. Strayer, C. Goumbala, and K. Gould (1993), Metabolism of streamwater dissolved organic carbon in the shallow hyporheic zone. Limnology and Oceanography, 38(**7**), 1493–1499, doi.org/10.4319/lo.1993.38.7.1493

Finlay, J. C. (2003), Controls of streamwater dissolved inorganic carbon dynamics in a forested watershed. Biogeochemistry, 62(**3**), 231-252. doi.org/10.1023/A:1021183023963

Fischer, H., S. C. Wanner, and M. Pusch (2002), Bacterial abundance and production in river sediments as related to the biochemical composition of particulate organic matter (POM). Biogeochemistry, 61(**1**), 37-55, doi.org/10.1023/A:1020298907014

Grimm, N. B., and S. G. Fisher (1984), Exchange between interstitial and surface water: Implications for stream metabolism and nutrient cycling. Hydrobiologia, 111(**3**), 219–228, doi.org/10.1007/BF00007202

Halpern, C. B., and J. F. Franklin (1990), Physiognomie development of Pseudotsuga forests in relation to initial structure and disturbance intensity. Journal of Vegetation Science, 1(**4**), 475-482, doi.org10.2307/3235781

Harvey, J. W., and K. E. Bencala (1993), The effect of streambed topography on surface-subsurface water exchange in mountain catchments. Water Resources Research, 29(**1**), 89-98, doi.org/10.1029/92WR01960

Hedin, L. O., J. C. von Fischer, N. E. Ostrom, B. P. Kennedy, M. G. Brown, and G. P. Robertson (1998), Thermodynamic constraints on nitrogentransformations and other biogeochemicalprocesses at soil–stream interfaces. Ecology, 79(**2**), 684-703, doi.org/10.1890/0012-9658(1998)079[0684:TCONAO]2.0.CO;2

Helton, A. M., M. S. Wright, E. S. Bernhardt, G. C. Poole, R. M. Cory, and J. A. Stanford (2015), Dissolved organic carbon lability increases with water residence time in the alluvial aquifer of a river floodplain ecosystem. Journal of Geophysical Research: Biogeosciences, 120(**4**), 693-706, doi.org/10.1002/2014JG002832

Johnson, M. S., J. Lehmann, S. J. Riha, A. V. Krusche, J. E. Richey, J. P. H. Ometto, and E. G. Couto, (2008), CO2 efflux from Amazonian headwater streams represents a significant fate for deep soil respiration. Geophysical Research Letters, 35(**17**), doi.org/10.1029/2008GL034619

Johnson, S., Wondzell, S., and Rothacher, J, (2020), Stream discharge in gaged watersheds at the HJ Andrews Experimental Forest, 1949 to present. Long-Term Ecological Research. Forest Science Data Bank, Corvallis, OR. [Database]. Available: http://andlter.forestry.oregonstate.edu/data/abstract.aspx?dbcode=HF004. https://doi.org/10.6073/pasta/0066d6b04e736af5f234d95d97ee84f3. Accessed 2021-02-09.

Jones, J. B., R. M. Holmes, S. G. Fisher, and N. B. Grimm (1994), Chemoautotrophic production and respiration in the hyporheic zone of a Sonoran Desert stream. Pages 329 – 338 in J.A. Stanford and H.M. Valett, editors. Proceeding of the Second International Conference on Ground Water Ecology. American Water Resources Association, Herndon, Virginia, USA.

Jones, J. B., S. G. Fisher, and N. B. Grimm (1995), Nitrification in the hyporheic zone of a desert stream ecosystem. Journal of the North American Benthological Society, 14(**2**), 249-258, doi.org/10.2307/1467777

Kasahara, T. (2000), Geomorphic controls on hyporheic exchange flow in mountain streams, Oregon. Corvallis, OR: Oregon State University. 103 p. MS thesis, Oreg. State Univ., Corvallis. [Available at https://ir.library.oregonstate.edu/concern/graduate_thesis_or_dissertations/0r9675820]

Kasahara, T., and S. M. Wondzell (2003), Geomorphic controls on hyporheic exchange flow in mountain streams. Water Resources Research, 39(**1**), SBH 3-1-SBH 3-14, doi.org/10.1029/2002wr001386

Lajtha, K., and J. Jones (2018), Forest harvest legacies control dissolved organic carbon export in small watersheds, western Oregon. Biogeochemistry, 140(**3**), 299-315, doi.org/10.1007/s10533-018-0493-3

Lee, B. S., and K. Lajtha (2016), Hydrologic and forest management controls on dissolved organic matter characteristics in headwater streams of old-growth forests in the Oregon Cascades. Forest Ecology and Management, 380, 11-22, doi.org/10.1016/j.foreco.2016.08.029

Levno, A., and J. Rothacher (1969), Increases in maximum stream temperatures after slash burning in a small experimental watershed. Res. Note PNW-RN-110. Portland, OR: US Department of Agriculture, Forest Service, Pacific Northwest Forest and Range Experiment Station. 7 p, 110. https://www.fs.fed.us/pnw/pubs/pnw_rn110.pdf

Malzone, J. M., S. K. Anseeuw, C. S. Lowry, C. S., and R. Allen-King (2016), Temporal hyporheic zone response to water table fluctuations. Groundwater, 54(**2**), 274-285, doi.org/10.1111/gwat.12352

Marx, A., J. Dusek, J. Jankovec, M. Sanda, T. Vogel, R. van Geldern, J. Hartmann and J. A. C. Barth (2017), A review of CO2 and associated carbon dynamics in headwater streams: A global perspective. Reviews of Geophysics, 55(**2**), 560–585, doi.org/10.1002/2016RG000547

Mermillod-Blondin, F., L. Mauclaire, and B. Montuelle (2005), Use of slow filtration columns to assess oxygen respiration, consumption of dissolved organic carbon, nitrogen transformations, and microbial parameters in hyporheic sediments. Water research, 39(**9**), 1687-1698, doi.org/10.1016/j.watres.2005.02.003

Metzler, G. M., and L. A. Smock (1990), Storage and dynamics of subsurface detritus in a sand-bottomed stream. Canadian Journal of Fisheries and Aquatic Sciences, 47(**3**), 588-594, doi.org/10.1139/f90-067

Palmer, S. M., D. Hope, M. F. Billett, J. J. C. Dawson, J. J. C., and C. L. Bryant (2001), Sources of organic and inorganic carbon in a headwater stream: Evidence from carbon isotope studies. Biogeochemistry, 52(3), 321–338, doi.org/10.1023/A:1006447706565

Pennington, R. S. (2019). Measurement of Gas Exchange, Stream Metabolism, and Carbon Fluxes of Headwater Streams. MS thesis, Oreg. State Univ., Corvallis. [Available at https://ir.library.oregonstate.edu/concern/graduate_thesis_or_dissertations/kh04dw66q]

Pett, R. J. (1989), Kinetics of microbial mineralization of organic carbon from detrital Skeletonema costatum cells. Marine ecology progress series. Oldendorf, 52(**2**), 123-128, http://www.jstor.org/stable/24833717

Pinheiro J, D. Bates, S. DebRoy, D. Sarkar, R Core Team (2020), _nlme: Linear and Nonlinear Mixed Effects Models_. R package version 3.1-149, https://CRAN.R-project.org/package=nlme

Pittroff, M., S. Frei, and B. S. Gilfedder (2017), Quantifying nitrate and oxygen reduction rates in the hyporheic zone using ^{222}Rn to upscale biogeochemical turnover in rivers. Water Resources Research, 53(**1**), 563-579, doi.org/10.1002/2016WR018917

Poole, G. C., J. A. Stanford, S. W. Running, and C. A. Frissell (2006), Multiscale geomorphic drivers of groundwater flow paths: subsurface hydrologic dynamics and hyporheic habitat diversity. Journal of the North American Benthological Society, 25(**2**), 288-303, doi.org/10.1899/0887-3593(2006)25[288:MGDOGF]2.0.CO;2

Pusch, M. (1996), The metabolism of organic matter in the hyporheic zone of a mountain stream, and its spatial distribution. Hydrobiologia, 323(**2**), 107–118, doi.org/10.1007/BF00017588

Reeder, W. J., A. M. Quick, T. B. Farrell, S. G. Benner, K. P. Feris, and D. Tonina (2018), Spatial and temporal dynamics of dissolved oxygen concentrations and bioactivity in the hyporheic zone. Water Resources Research, 54(**3**), 2112-2128, doi.org/10.1002/2017WR021388

Richardson, J. S., & Danehy, R. J. (2007), A synthesis of the ecology of headwater streams and their riparian zones in temperate forests. Forest Science, 53(**2**), 131-147, doi.org/10.1093/forestscience/53.2.131

Rodrigues, R. M. N. V., and P. J. L. B. Williams (2001), Heterotrophic bacterial utilization of nitrogenous and nonnitrogenous substrates, determined from ammonia and oxygen fluxes. Limnology and Oceanography, doi.org/10.4319/lo.2001.46.7.1675

Rothacher, J., C. T. Dyrness, and R. L. Fredriksen (1967), Hydrologic and related characteristics of three small watersheds in the Oregon Cascades. Portland, OR: U.S. Department of Agriculture, Forest Service, Pacific Northwest Forest and Range Experiment Station. 54 p. https://andrewsforest.oregonstate.edu/publications/344

Rounds, S. A., F. D. Wilde, and G. F. Ritz (2006), Chapter A6. Section 6.2. Dissolved oxygen. Techniques of Water-Resources Investigations, doi.org/10.3133/twri09A6.2

Rovira, P., and R. Rovira (2010), Fitting litter decomposition datasets to mathematical curves: towards a generalised exponential approach. Geoderma, 155(**3-4**), 329-343, doi.org/10.1016/j.geoderma.2009.11.033

Schindler, J. E., and D. P. Krabbenhoft (1998), The hyporheic zone as a source of dissolved organic carbon and carbon gases to a temperate forested stream. Biogeochemistry, 43(**2**), 157–174, doi.org/10.1023/A:1006005311257

Shibata, H., H. Mitsuhashi, Y. Miyake, and S. Nakano (2001), Dissolved and particulate carbon dynamics in a cool-temperate forested basin in northern Japan. Hydrological Processes, 15(**10**), 1817-1828, doi.org/10.1002/hyp.241

Sobczak, W. V., and S. Findlay (2002), Variation in Bioavailability of Dissolved Organic Carbon among Stream Hyporheic flow paths. Ecology, 83(**11**), 3194, doi.org/10.2307/3071853

Stegen, J. C., J. K. Fredrickson, M. J. Wilkins, A. E. Konopka, W. C. Nelson, E. V. Arntzen, W. B. Chrisler, R. K. Chu, R E. Danczak, S . J. Fansler, D. W. Kennedy, C. T. Resch, and M. Tfaily (2016), Groundwater–surface water mixing shifts ecological assembly processes and stimulates organic carbon turnover. Nature communications, 7, 11237, doi.org/10.1038/ncomms11237

Swanson, F. J., and M. E. James (1975), Geology and geomorphology of the H.J. Andrews Experimental Forest, Western Cascades, Oregon. Res. Pap. PNW-188.

Tsypin, M., and G. L. Macpherson (2012), The effect of precipitation events on inorganic carbon in soil and shallow groundwater, Konza Prairie LTER Site, NE Kansas, USA.

Applied geochemistry, 27(**12**), 2356-2369, doi.org/10.1016/j.apgeochem.2012.07.008

Vieweg, M., M. J. Kurz, N. Trauth, J. H. Fleckenstein, A. Musolff, and C. Schmidt (2016), Estimating time-variable aerobic respiration in the streambed by combining electrical conductivity and dissolved oxygen time series. Journal of Geophysical Research: Biogeosciences, 121(**8**), 2199-2215, doi/10.1002/2016JG003345.

Voltz, T., M. Gooseff, A. S. Ward, K. Singha, M. Fitzgerald, and T. Wagener, (2013), Riparian hydraulic gradient and stream-groundwater exchange dynamics in steep headwater valleys. Journal of Geophysical Research: Earth Surface, 118(**2**), 953-969, doi.org/10.1002/jgrf.20074

Wagner, K., M. M. Bengtsson, K. Besemer, A. Sieczko, N. R. Burns, E. R. Herberg, and T. J. Battin (2014), Functional and structural responses of hyporheic biofilms to varying sources of dissolved organic matter. Applied and environmental microbiology, 80(**19**), 6004-6012, doi.org/10.1128/AEM.01128-14

Ward, A. S., N. M. Schmadel, S. M. Wondzell, C. Harman, M. N. Gooseff, and K. Singha (2016), Hydrogeomorphic controls on hyporheic and riparian transport in two headwater mountain streams during base flow recession. Water Resources Research, 52(**2**), 1479-1497, doi.org/10.1002/2015WR018225

Wilson, H. F., P. A. Raymond, J. E. Saiers, W. V. Sobczak and N. Xu (2016), Increases in humic and bioavailable dissolved organic matter in a forested New England headwater stream with increasing discharge. Marine and Freshwater Research, 67(**9**), 1279-1292, doi.org/10.1071/MF15286

Wondzell, S. M. (2006), Effect of morphology and discharge on hyporheic exchange flows in two small streams in the Cascade Mountains of Oregon, USA. Hydrological Processes: An International Journal, 20(**2**), 267-287, doi.org/10.1002/hyp.5902

Wondzell, S. M., and F. J. Swanson (1996), Seasonal and storm dynamics of the hyporheic zone of a 4th-order mountain stream. I: Hydrologic processes. Journal of the North American Benthological Society, 15(**1**), 3-19, doi.org/10.2307/1467429

Wondzell, S. M., and F. J. Swanson (1999), Floods, channel change, and the hyporheic zone. Water Resources Research, 35(**2**), 555-567, doi.org/10.1029/1998WR900047

Wondzell, S. M., and M. N. Gooseff (2013), Geomorphic controls on hyporheic exchange across scales - Watersheds to particles, in Treatise on Geomorphology, edited by J. Shroder and E. Wohl, Vol. 9, pp. 203– 218. Academic Press, San Diego, Calif.

APPENDICES

Appendix A Supplementary Figures

Figure A.1 – Pictures of hyporheic mesocosm located in Watershed 1. Hyporheic mesocosm facility is adjacent to the gage house. Top two pictures show aluminum clam shell in closed position.

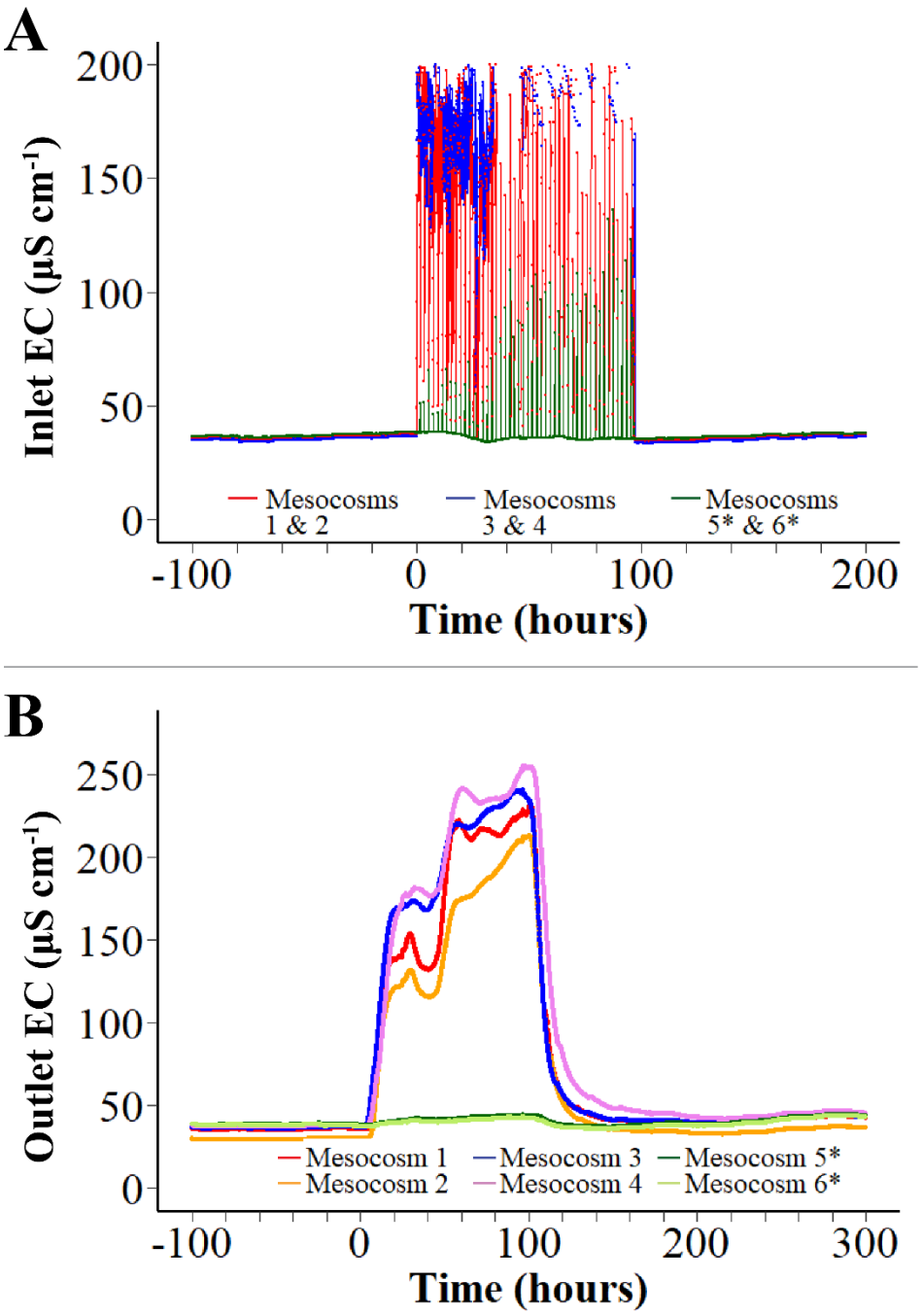

Figure A.2 – Breakthrough curves of electrical conductivity measured at the inlet (A) and the outlet (B) from 2nd NaCl tracer injection experiment conducted from 04/23/2017 to 04/27/2017. Mesocosms with * are control mesocosms that did not receive tracer treatments.

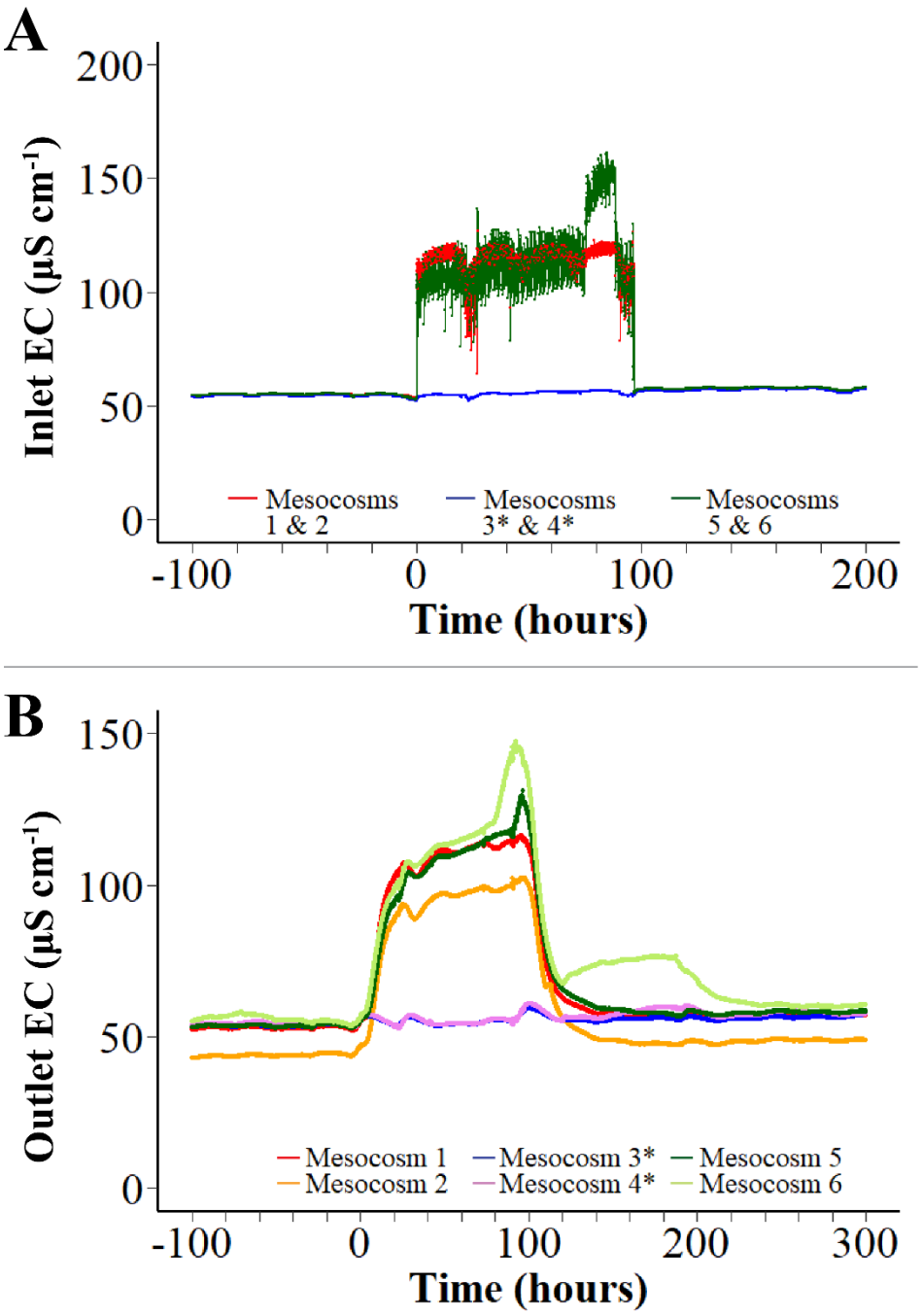

Figure A.3 – Breakthrough curves of electrical conductivity measured at the inlet (A) and the outlet (B) from 3rd NaCl tracer injection experiment conducted from 07/29/2017 to 08/02/2017. Mesocosms with * are control mesocosms that did not receive tracer treatments.

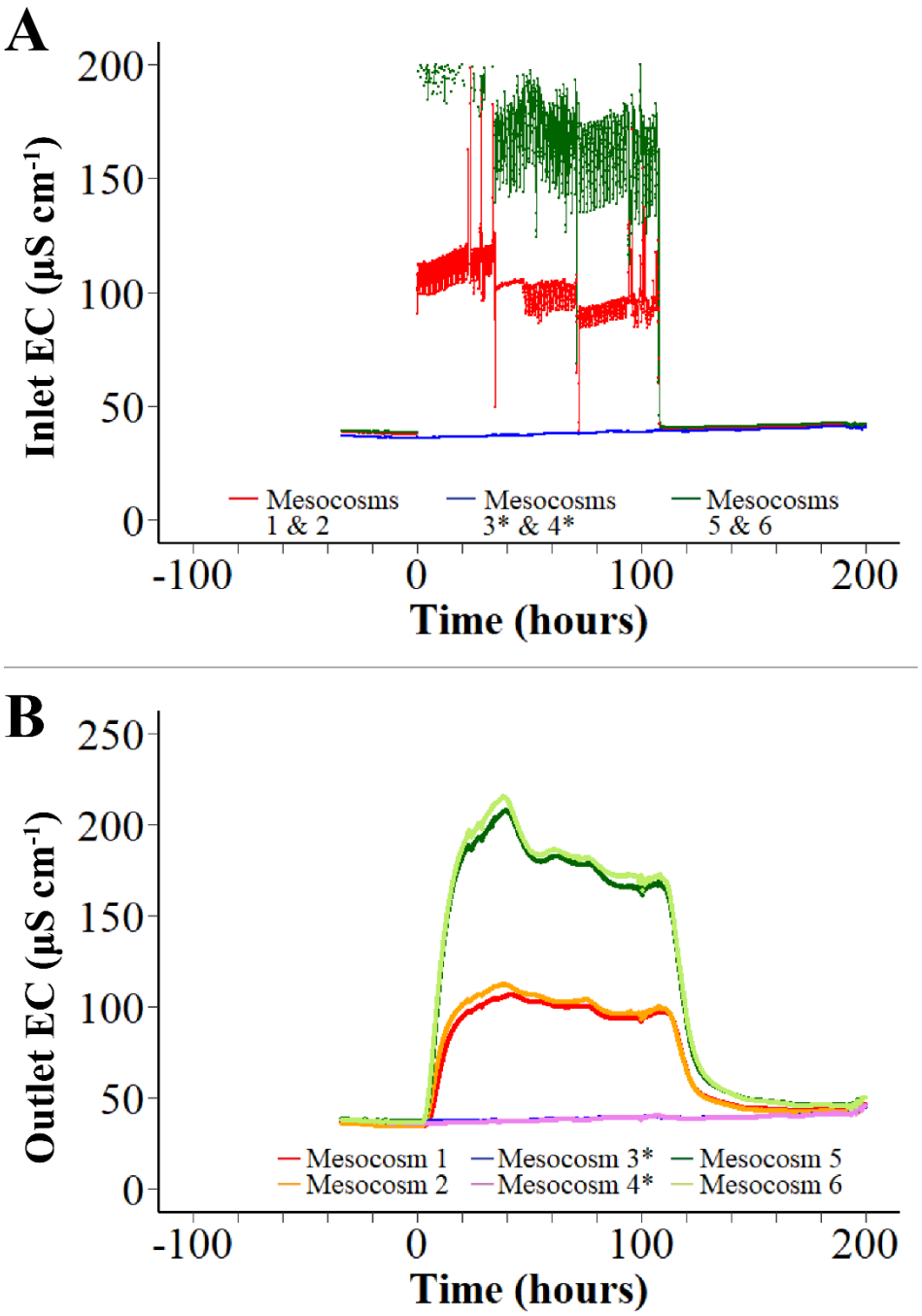

Figure A.4 – Breakthrough curves of electrical conductivity measured at the inlet (A) and the outlet (B) from 4th NaCl tracer injection experiment conducted from 04/17/2018 to 04/21/2018. Mesocosms with * are control mesocosms that did not receive tracer treatments.

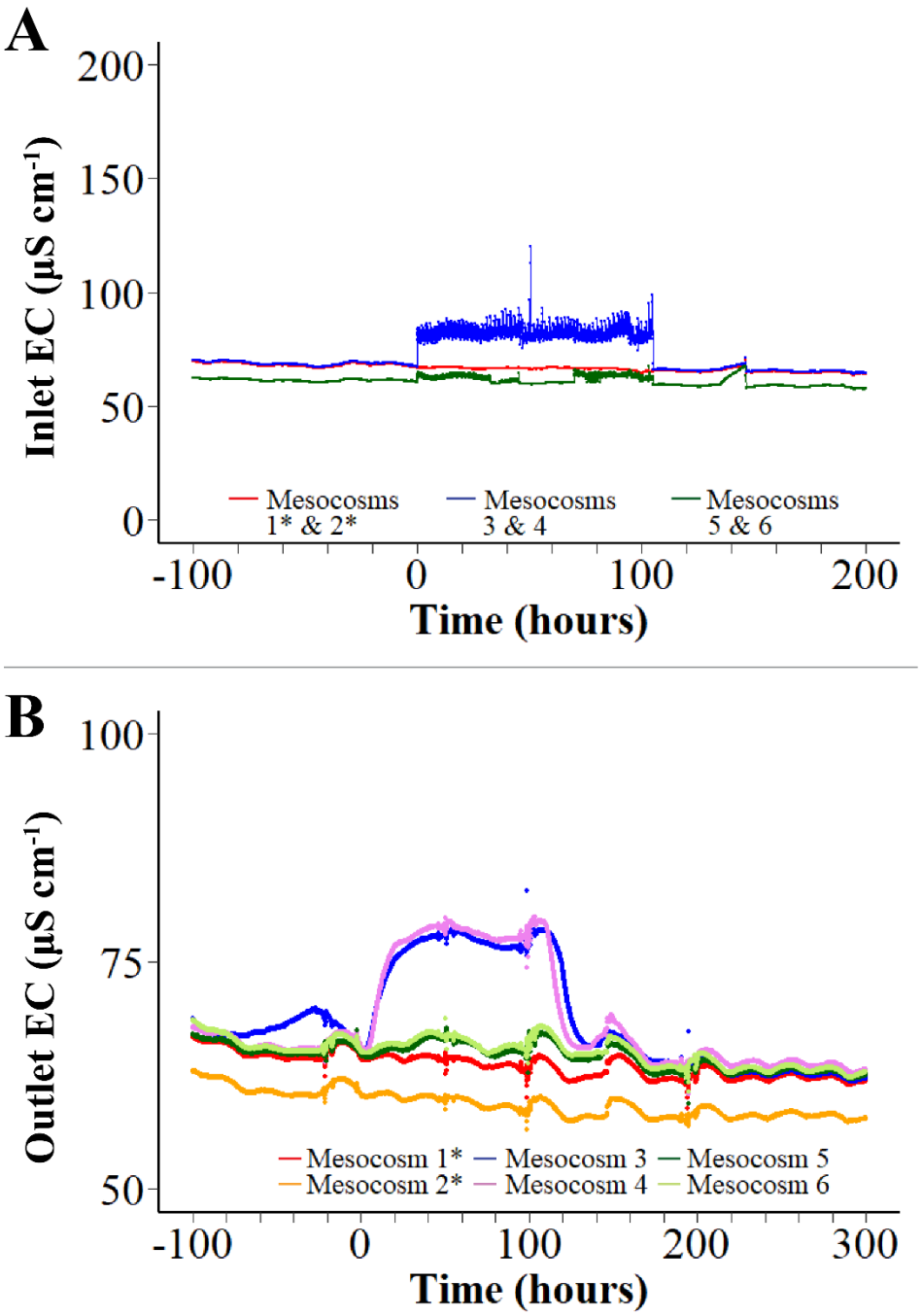

Figure A.5 – Breakthrough curves of electrical conductivity measured at the inlet (A) and the outlet (B) from 5th NaCl tracer injection experiment conducted from 08/28/2018 to 09/02/2018. Mesocosms with * are control mesocosms that did not receive tracer treatments.

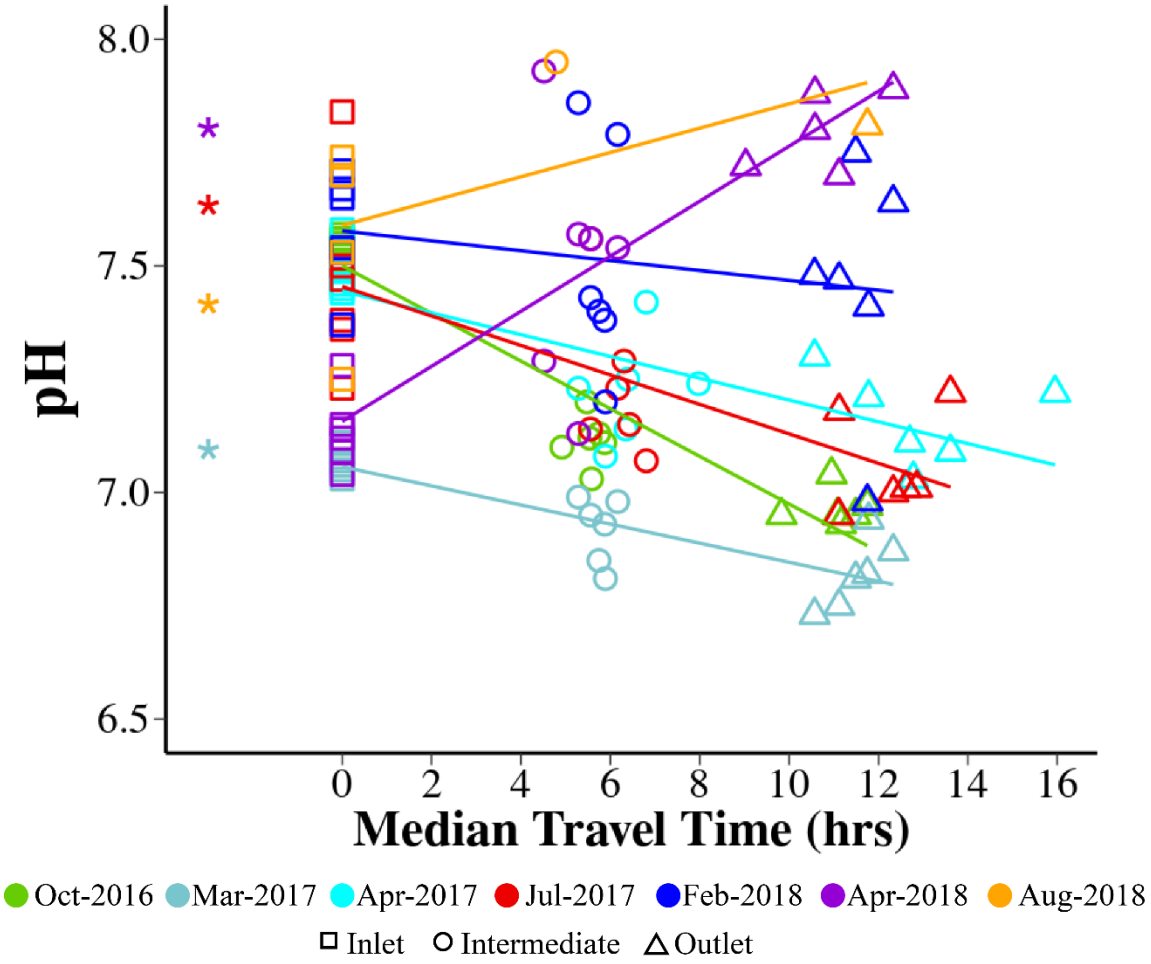

Figure A.6 – Patterns of pH across 2 m hyporheic flow paths of mesocosms.

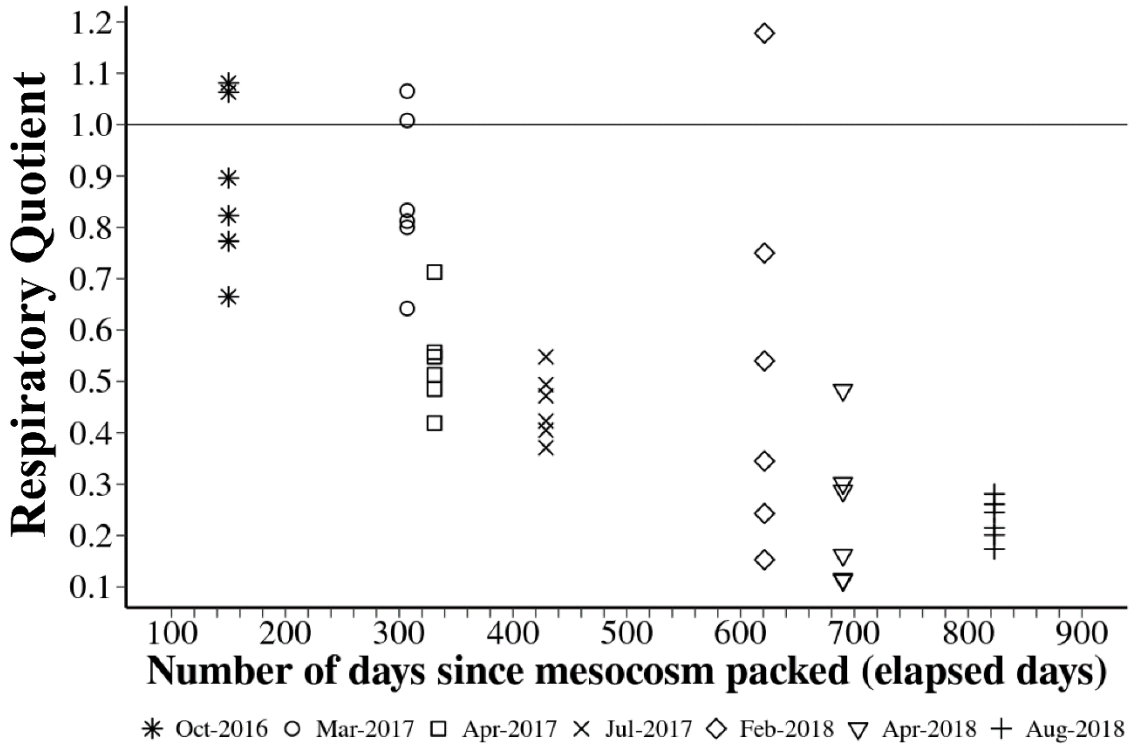

Figure A.7 – Respiratory quotient (RQ) over time in the hyporheic mesocosms. The RQ is a dimensionless number calculated from molar ratio of $|\Delta DIC|$ to $|\Delta O_2|$. The RQ of 1 represents 1 mole of DIC produced for 1 mole of O_2 consumed.

Appendix B Supplementary Tables

Table B.1– Results of paired two sample t tests of dissolved organic carbon (DOC) sampled from hyporheic mesocosms inlets using two different sample collection methods: old method (syringe-method) and new method (sample-jar collection method).

	Old Method	New Method
Inlets	0.065	0.065
	0.063	0.067
	0.065	0.065
	0.067	0.076
	0.066	0.066
	0.065	0.063

t-Test: Paired Two Sample for Means

	Old Method	*New Method*
Mean	0.065268203	0.066946009
Variance	1.39695E-06	2.23129E-05
Observations	6	6
Pearson Correlation	0.471945017	
Hypothesized Mean Difference	0	
df	5	
t Stat	-0.957053207	
P(T<=t) one-tail	0.191246778	
t Critical one-tail	2.015048373	
P(T<=t) two-tail	0.382493557	
t Critical two-tail	2.570581836	

Table B.2 – Results of paired two sample t tests of dissolved organic carbon (DOC) sampled from hyporheic mesocosms intermediates using two different sample collection methods: old method (syringe-method) and new method (sample-jar collection method).

	Old Method	**New Method**
Intermediates	0.064	0.064
	0.065	0.061
	0.065	0.064
	0.062	0.062
	0.061	0.063
	0.064	0.072

t-Test: Paired Two Sample for Means

	Old Method	*New Method*
Mean	0.063510947	0.0645582
Variance	2.71015E-06	1.5968E-05
Observations	6	6
Pearson Correlation	0.184444177	
Hypothesized Mean Difference	0	
df	5	
t Stat	-0.636328168	
P(T<=t) one-tail	0.276273735	
t Critical one-tail	2.015048373	
P(T<=t) two-tail	0.55254747	
t Critical two-tail	2.570581836	

Table B.3 – Results of paired two sample t tests of dissolved organic carbon (DOC) sampled from hyporheic mesocosms outlets using two different sample collection methods: old method (syringe-method) and new method (sample-jar collection method).

	Old Method	New Method
Outlets	0.059	0.062
	0.065	0.061
	0.063	0.061
	0.058	0.059
	0.060	0.062
	0.062	0.063

t-Test: Paired Two Sample for Means

	Old Method	*New Method*
Mean	0.061106088	0.061338977
Variance	8.5383E-06	2.15568E-06
Observations	6	6
Pearson Correlation	0.29195636	
Hypothesized Mean Difference	0	
df	5	
t Stat	-0.199348524	
P(T<=t) one-tail	0.424921739	
t Critical one-tail	2.015048373	
P(T<=t) two-tail	0.849843478	
t Critical two-tail	2.570581836	

Table B.4 – Results of mixed-effects model of k_{O_2} without correlation structure.

Full model k_{O_2} = average temperature + season + elapsed days + inletDOC

Linear mixed-effects model fit by REML

AIC	BIC	logLik
-196.5017	-185.2252	105.2508

Random effects:

Formula: ~1 | factor.mesocosm

	(Intercept)	Residual
StdDev:	3.243745e-07	0.01062398

Fixed effects:

	Value	Std. Error	DF	t-value	p-value
Intercept	0.01752704	0.03310110	32	0.5295003	0.6001
Avg. Temp	0.00090282	0.00116789	32	0.7730392	0.4452
Season	-0.02301751	0.00800525	32	-2.8753026	0.0071
Elapsed days	0.00000518	0.00001145	32	0.4528579	0.6537
Inlet DOC	0.08925589	0.16463420	32	0.5421467	0.5915

Table B.5 – Results of mixed-effects model of k_{O_2} with Gaus correlation structure.

Full model k_{O_2} = average temperature + season + elapsed days + inletDOC

Linear mixed-effects model fit by REML

AIC	BIC	logLik
-213.6093	-191.0564	120.8046

Random effects:

Formula: ~1 | factor.mesocosm

	(Intercept)	Residual
StdDev:	3.343207e-07	0.00273169

Correlation Structure: Gaussian spatial correlation

Formula: ~integer.elsdays | factor.mesocosm

Parameter estimate(s):

range	nugget
4.884325e+01	1.765474e-15

Fixed effects:

	Value	Std. Error	DF	t-value	p-value
Intercept	0.04486977	0.01396437	32	3.213162	0.0030
Avg. Temp	0.00015352	0.00057156	32	0.268596	0.7900
Season	-0.02615039	0.00434360	32	-6.020437	0.0000
Elapsed days	-0.00001174	0.00000471	32	-2.494183	0.0180
Inlet DOC	-0.04218120	0.06007772	32	-0.702110	0.4877

Table B.6 – Results of mixed-effects model of k_{O_2} with Exponential Spatial correlation structure.

Full model k_{O_2} = average temperature + season + elapsed days + inletDOC

Linear mixed-effects model fit by REML

AIC	BIC	logLik
-212.5945	-190.0417	120.2973

Random effects:

Formula: ~1 | factor.mesocosm

	(Intercept)	Residual
StdDev:	3.750018e-07	0.00284842

Correlation Structure: Exponential spatial correlation

Formula: ~integer.elsdays | factor.mesocosm

Parameter estimate(s):

range	nugget
5.482242e+01	1.701598e-13

Fixed effects:

	Value	Std. Error	DF	t-value	p-value
Intercept	0.04167597	0.01489557	32	2.797877	0.0086
Avg. Temp	0.00022903	0.00059410	32	0.385507	0.7024
Season	-0.02572241	0.00434884	32	-5.914777	0.0000
Elapsed days	-0.00001059	0.00000507	32	-2.089563	0.0447
Inlet DOC	-0.02193294	0.06792936	32	-0.322879	0.7489

Table B.7 – Results of mixed-effects model of k_{DIC} without correlation structure.

Full model k_{DIC} = average temperature + season + elapsed days + inletDOC

Linear mixed-effects model fit by REML

AIC	BIC	logLik
-325.439	-314.1626	169.7195

Random effects:

Formula: ~1 | factor.mesocosm

	(Intercept)	Residual
StdDev:	0.0004492001	0.001816094

Fixed effects:

	Value	Std. Error	DF	t-value	p-value
Intercept	0.02371910	0.005672211	32	4.181633	0.0002
Avg. Temp	-0.00051595	0.000199961	32	-2.580242	0.0147
Season	-0.00813529	0.001370078	32	-5.937834	0.0000
Elapsed days	-0.00001799	0.000001959	32	-9.186010	0.0000
Inlet DOC	0.03567602	0.028200010	32	1.265107	0.2150

Table B.8 – Results of mixed-effects model of k_{DIC} without Linear spatial correlation structure.

Full model k_{DIC} = average temperature + season + elapsed days + inletDOC

Linear mixed-effects model fit by REML

AIC	BIC	logLik
-324.6209	-302.068	176.3104

Random effects:

Formula: ~1 | factor.mesocosm

(Intercept)	Residual
StdDev: 0.0004830817	0.0002851231

Correlation Structure: Linear spatial correlation

Formula: ~integer.elsdays | factor.mesocosm

Parameter estimate(s):

range	nugget
53.41829773	0.07724512

Fixed effects:

	Value	Std. Error	DF	t-value	p-value
Intercept	0.02103910	0.002140757	32	9.827881	0
Avg. Temp	-0.00053781	0.000079305	32	-6.781575	0
Season	-0.00858206	0.000589000	32	-14.570575	0
Elapsed days	-0.00001667	0.000000662	32	-25.171324	0
Inlet DOC	0.06427416	0.010039651	32	6.402031	0

Table B.9 – Results of mixed-effects model of k_{DIC} without Gaussian spatial correlation structure.

Full model k_{DIC} = average temperature + season + elapsed days + inletDOC

Linear mixed-effects model fit by REML

AIC	BIC	logLik
-324.6102	-302.0573	176.3051

Random effects:

Formula: ~1 | factor.mesocosm

(Intercept)	Residual
StdDev: 0.0004835871	0.000282929

Correlation Structure: Gaussian spatial correlation

Formula: ~integer.elsdays | factor.mesocosm

Parameter estimate(s):

range	nugget
2.854933e+01	4.239440e-07

Fixed effects:

	Value	Std. Error	DF	t-value	p-value
Intercept	0.02099237	0.002134337	32	9.835548	0
Avg. Temp	-0.00053649	0.000078884	32	-6.801033	0
Season	-0.00857333	0.000584903	32	-14.657703	0
Elapsed days	-0.00001666	0.000000660	32	-25.254722	0
Inlet DOC	0.06455062	0.010031175	32	6.435001	0

Table B.10 – Results of mixed-effects model of k_{DIC} without Exponential spatial correlation structure.

Full model k_{DIC} = average temperature + season + elapsed days + inletDOC

AIC	BIC	logLik
-324.3328	-301.78	176.1664

Random effects:

Formula: ~1 | factor.mesocosm

(Intercept)	Residual
StdDev: 0.0004919526	0.00026273

Correlation Structure: Exponential spatial correlation

Formula: ~integer.elsdays | factor.mesocosm

Parameter estimate(s):

range	nugget
2.064260e+01	1.123603e-07

Fixed effects:

	Value	Std. Error	DF	t-value	p-value
Intercept	0.02051317	0.002067754	32	9.920506	0
Avg. Temp	-0.00052291	0.000074677	32	-7.002243	0
Season	-0.00848305	0.000543229	32	-15.615964	0
Elapsed days	-0.00001654	0.000000635	32	-26.041315	0
Inlet DOC	0.06739071	0.009912923	32	6.798269	0

Table B.11 – Results of mixed-effects model of k_{DIC} without Spherical spatial correlation structure.

Full model k_{DIC} = average temperature + season + elapsed days + inletDOC

Linear mixed-effects model fit by REML

AIC BIC logLik

-324.6205 -302.0677 176.3103

Random effects:

Formula: ~1 | factor.mesocosm

(Intercept) Residual

StdDev: 0.0004841515 0.0002838698

Correlation Structure: Spherical spatial correlation

Formula: ~integer.elsdays | factor.mesocosm

Parameter estimate(s):

range nugget

6.925939e+01 8.728410e-07

Fixed effects:

	Value	Std. Error	DF	t-value	p-value
Intercept	0.02101670	0.002136605	32	9.836494	0
Avg. Temp	-0.00053718	0.000079051	32	-6.795293	0
Season	-0.00857785	0.000586694	32	-14.620656	0
Elapsed days	-0.00001667	0.000000661	32	-25.223975	0
Inlet DOC	0.06440960	0.010030919	32	6.421106	0